SPECTRAL PROPERTIES OF X-RAY BINARIES IN CENTAURUS A

MARK J. BURKE[1,2], SOMAK RAYCHAUDHURY[1,15], RALPH P. KRAFT[2], THOMAS J. MACCARONE[9], NICOLA J. BRASSINGTON[3],
MARTIN J. HARDCASTLE[3], JOUNI KAINULAINEN[7], KRISTIN A. WOODLEY[5,16], JOANNA L. GOODGER[3], GREGORY R. SIVAKOFF[4],
WILLIAM R. FORMAN[2], CHRISTINE JONES[2], STEPHEN S. MURRAY[5,2], MARK BIRKINSHAW[8,2], JUDITH H. CROSTON[9],
DANIEL A. EVANS[2], MARAT GILFANOV[10,14], ANDRÉS JORDÁN[2,11], CRAIG L. SARAZIN[12], RASMUS VOSS[13], DIANA M. WORRALL[8,2],
AND ZHONGLI ZHANG[10]

Draft version February 6, 2013

ABSTRACT

We present a spectral investigation of X-ray binaries in NGC 5128 (Cen A), using six 100 ks *Chandra* observations taken over two months in 2007. We divide our sample into thermally and non-thermally dominated states based on the behavior of the fitted absorption column N_H, and present the spectral parameters of sources with $L_x \gtrsim 2 \times 10^{37}$ erg s^{-1}. The majority of sources are consistent with being neutron star low mass X-ray binaries (NS LMXBs) and we identify three transient black hole (BH) LMXB candidates coincident with the dust lane, which is the remnant of a small late-type galaxy. Our results also provide tentative support for the apparent 'gap' in the mass distribution of compact objects between $\sim 2-5\,M_\odot$.

We propose that BH LMXBs are preferentially found in the dust lane, and suggest this is because of the younger stellar population. The majority ($\sim 70-80\%$) of potential Roche-lobe filling donors in the Cen A halo are $\gtrsim 12$ Gyr old, while BH LMXBs require donors $\gtrsim 1 M_\odot$ to produce the observed peak luminosities. This requirement for more massive donors may also explain recent results that claim a steepening of the X-ray luminosity function with age at $L_x \geq 5 \times 10^{38}$ erg s^{-1} for the XB population of early-type galaxies; for older stellar populations, there are fewer stars $\gtrsim 1 M_\odot$, which are required to form the more luminous sources.

Subject headings: galaxies: elliptical and lenticular, cD — galaxies: individual (Centaurus A, NGC 5128) — X-rays: galaxies — X-rays: binaries

1. INTRODUCTION

Population studies of extragalactic X-ray binaries (XBs) located beyond the Local Group have been made possible thanks to the excellent sensitivity and spatial resolution of the *Chandra* X-ray observatory (Weisskopf et al. 2000). For over a decade, astronomers have resolved the hard X-ray spectral

[1] School of Physics and Astronomy, University of Birmingham, Edgbaston, Birmingham, B15 2TT, UK

[2] Harvard-Smithsonian Center for Astrophysics, 60 Garden Street, Cambridge, MA 02138, USA

[3] School of Physics, Astronomy, and Mathematics, University of Hertfordshire, Hatfield, AL10 9AB, UK

[4] Department of Physics, University of Alberta, Edmonton, Alberta T6G 2E1, Canada

[5] Department of Physics and Astronomy, University of British Columbia, Vancouver BC V6T 1Z1, Canada

[6] Department of Physics and Astronomy, Johns Hopkins University, 3400 N. Charles Street, Baltimore, MD 21218, USA

[7] Max-Planck-Institute for Astronomy, Königstuhl 17, 69117 Heidelberg,Germany

[8] HH Wills Physics Laboratory, University of Bristol, Tyndall Avenue, Bristol BS8 1TL, UK

[9] School of Physics and Astronomy, University of Southampton, Southampton, SO17 1BJ, UK

[10] Max Planck Institut für Astrophysik, Karl-Schwarzschild-Str. 1, D-85741, Garching, Germany

[11] Departamento de Astronomía y Astrofísica, Pontificia Universidad Católica de Chile, Casilla 306, Santiago 22, Chile

[12] Department of Astronomy, University of Virginia, P.O. Box 400325, Charlottesville, VA 22904-4325, USA

[13] Department of Astrophysics/IMAPP, Radboud, University Nijmegen, PO Box 9010, NL-6500 GL Nijmegen, the Netherlands.

[14] Space Research Institute, Russian Academy of Sciences, Profsoyuznaya 84/32, 117997 Moscow, Russia

[15] Department of Physics, Presidency University, Kolkata 700 073, India

[16] UC Santa Cruz, University of California Observatories, 1156 High Street, Santa Cruz, CA 95064, USA

component of galaxies at sub-arcsecond precision into predominantly non-nuclear point sources (Sarazin et al. 2000). Much research has focused on associations with globular clusters, which contain the majority of X-ray point sources in some elliptical galaxies (e.g. Angelini et al. 2001). It has been observed that metal rich clusters are clearly favored as the hosts of X-ray sources (Kundu et al. 2002) and that the densest clusters preferentially host X-ray sources (Jordán et al. 2007). Ultraluminous X-ray sources, which display isotropic luminosities $L_x > 10^{39}$ erg s^{-1} (Fabbiano 1989), have been studied in great detail by both *Chandra* and *XMM-Newton*. Optical observations have been used to detect counterparts for these sources in star-forming galaxies (Roberts et al. 2008), and to demonstrate association with globular clusters in a few early-type galaxies (e.g. Maccarone et al. 2007; Brassington et al. 2012).

The X-ray luminosity function (XLF) is a well-studied statistical characteristic of the X-ray source population for a given galaxy. Grimm et al. (2002) conducted a study of Galactic XBs and found that the XLF of high-mass X-ray binaries (HMXBs) tightly follows a power law above 10^{37} erg s^{-1}, while that of low-mass X-ray binaries (LMXBs) experiences a sharp cut-off above a few 10^{38} erg s^{-1}. Usually there are too few counts to derive the source spectra directly and XLFs are produced using an assumed spectrum, typically a power law with $\Gamma \sim 1.5-1.7$, which approximates the emission from Galactic XBs. An LMXB population dominates the XLF of discrete sources in early-type galaxies (see Fabbiano 2006, for review), due to their older stellar population; early-type galaxies contain relatively few high luminosity($> 10^{38}$ erg s^{-1}) sources compared to late-type star-forming galaxies.

The tendancy of LMXBs to dominate the discrete source

XLFs in early-type galaxies can be linked to the study of XB populations in late-type galaxies, where two distinct populations have been observed (Prestwich et al. 2009). One population, associated primarily with the bulge, follows an XLF that steepens after a few $\times 10^{38}$ erg s^{-1}, while the other population is associated with the spiral arms and has an XLF consistent with that of HMXBs. The latter population has both softer colours and higher luminosities than Galactic, wind-driven HMXBs, most of which are accretion-powered pulsars with high magnetic fields, and the spectra are well-described by relatively cool disk blackbodies (0.1-1.1 keV), suggesting that they too are Roche-lobe-filling accretion driven systems.

A luminosity break at $L_x \sim 2.5 - 5.0 \times 10^{38}$ erg s^{-1} has been seen in the discrete source population of numerous early-type galaxies (e.g., Sarazin et al. 2001) and is potentially the Eddington-limited extent of the brightest neutron star (NS) LMXBs. The brightest sources are super-Eddington for a 1.4 M$_\odot$ NS and are probably BH XRBs or the more massive extreme of the NS LMXB population. The luminosity break was examined in detail over a sample of nearby elliptical galaxies by Kim & Fabbiano (2010), who found that the lack of sources with $L_x > 5 \times 10^{38}$ erg s^{-1} was more pronounced for older (> 5 Gyr) galaxies. The observed steepening of the break in the XLF suggests that young early-type XB populations are intermediate in nature between those of star-forming galaxies and old early-types.

NGC 5128 (Centaurus A) is the nearest optically luminous early-type galaxy, at a distance of 3.7 Mpc (Ferrarese et al. 2007), with $M_B = -21.1$. A small late-type galaxy is currently merging with Cen A (Graham 1979); however, the galaxies remain poorly mixed (Quillen et al. 2006). The central regions of the galaxy are notable for the presence of vast dust lanes that contain many active star forming regions. Rejkuba et al. (2011) compared simulated color-magnitude diagrams with deep ACS/HST photometry and concluded that *at least* 70% of stars in NGC 5128 formed 12 ± 1 Gyr ago and a smaller population of more metal rich stars formed in the last 2-4 Gyr. Therefore we expect the population of XBs to be dominated by LMXBs that possess old main sequence companions of $M < 1$M$_\odot$ with the potential for a small component from LMXBs with more massive companions.

Six 100 ks *Chandra* observations of NGC 5128 were taken as part of the Cen A Very Large Project (VLP) spanning the course of 2 months in 2007 (Jordán et al. 2007). These observations led to investigation of the source's striking X-ray features such as the AGN jet (Hardcastle et al. (2007), Worrall et al. (2008), Goodger et al. (2010)), radio-lobe shock (Croston et al. 2009) and the extended gaseous emission (Kraft et al. 2008). The relationship between XBs and globular clusters was investigated by Voss et al. (2009), who confirmed the presence of a low-luminosity break in the XLF at $L_x \sim 1.5 - 4 \times 10^{37}$ erg s^{-1} and a lack of GC sources with $L_x < 3 \times 10^{36}$ erg s^{-1}. Voss et al. (2009) suggested that this dearth of faint sources may indicate that GC LMXB companions are He rich, which possess a larger critical mass accretion rate $\dot{M}_{crit}$ to become transients. Sources approaching the corresponding luminosity to $\dot{M}_{crit}$ become unstable, and are therefore always above or below this luminosity, leaving a gap in the XLF. However, it now appears more likely that the low-luminosity break results from a change in the disk instability criterion at low accretion rates as the disk spectrum peaks at longer wavelengths (van Haaften et al. 2012). These Cen A data were also used by Zhang et al. (2011) as part of

a large sample of GC-LMXBs from many elliptical galaxies, and discrepancies between the GC and field XLFs were found across $L_x \sim 10^{36} - 10^{39}$ erg s^{-1}.

The current era of deep X-ray observations has enabled more detailed study of individual XBs beyond the Local Group. Brassington et al. (2010) and Fabbiano et al. (2010) present the results of spectral fitting the brightest sources in the early-type galaxies NGC 3379 and NGC 4278, down to a limiting unabsorbed luminosity of $\sim 1.2 \times 10^{38}$ erg s^{-1}. These samples contained 8 and 7 XBs, respectively, of which 7 were coincident with globular clusters (GCs). These works adopted a diagnostic approach to spectral fitting, inferring the state of a source based on fitting simple spectral models, a multi-colored disk blackbody and power law. The true state of the source can be inferred from the behavior of the absorption parameter N_H, which simulations showed to behave in a characteristic way depending on the true state of the source. This method essentially assesses the relative contribution of thermal and non-thermal emission to the spectrum, and is fully described by Brassington et al. (2010) (see section 3.2). A further study of 18 transient-type sources from galaxies NGC 3379, NGC 4278 and NGC 4697 by Brassington et al. (2012) found a host of exotic sources, including a GC ULX in outflow and an unusually luminous bursting source. They distinguished spectral states down to $\sim 10^{38}$ erg s^{-1}.

In Cen A we expect to detect both neutron star (NS) and black hole (BH) XBs, both of which can be transients. It is generally thought that the transient behavior occurs due to the disk ionization instability mechanism (DIM), which was first developed for explaining the dwarf nova outbursts of cataclysmic variables (Smak 1984). The essential feature of this model is that the viscosity of ionized gas is larger than that of neutral gas. Its application to X-ray binaries is complicated by irradiation of the outer accretion disk, which is a considerably more important factor (Dubus et al. 2001). Recently, Coriat et al. (2012) tested the DIM with a population of Galactic sources, finding that the critical mass accretion rate above which sources are persistent is lower than that predicted when irradiation is not taken into account. Black holes are more massive than neutron stars, but have similar radiative efficiencies, and a consequence is that the outer disk temperatures for black hole X-ray binaries at a given orbital period will be smaller than those for neutron star X-ray binaries; thus black hole systems are far more likely to be transient than are neutron star systems (King et al. 1996).

An empirical understanding of the properties of transient X-ray binaries has started to develop. The size of the accretion disk should determine the peak outburst luminosity (e.g. Shahbaz et al. 1998), and this has been borne out as large samples of such transient outbursts have developed (Portegies Zwart et al. (2004); Wu et al. (2010)). As sources change in luminosity, they follow loops in a hardness-intensity diagram (Maccarone & Coppi 2003), indicating that they are changing spectral shapes hysteretically. In general, the spectral changes occur rapidly, with X-ray binaries in outburst spending most of their time in just a few spectral states. Remillard & McClintock (2006) posit that BH LMXBs possess spectra characterized by three key spectral states. The thermal-dominant state, where the emission appears to be dominated by a ~ 1 keV multicolor disk blackbody, is essentially the same as the standard geometrically thin, optically thick accretion disk of Shakura & Sunyaev (1973). During the ingress and egress of outburst, the source experiences

a hard power-law state of $\Gamma \sim 1.7$, the emission likely due to inverse Compton scattering in an optically thin, geometrically thick region (Thorne & Price 1975). Near the peak of outburst, some sources also exhibit a steep power law state $\Gamma \sim 2.5$ extending to MeV energies with a significant thermal component also present. These spectral states are also associated with the rapid variability of the sources (Homan et al. 2001) and changes in the radio jet properties (Fender et al. 2004).

NS LMXBs generally show similar spectral state phenomenology to BH systems (van der Klis 1994), but have some differences since the NS surface provides a boundary layer. Nonetheless, in both cases, low/hard type spectra are typically seen below $\sim 2\%$ of the Eddington luminosity, except during the hysteretic intervals near the beginning of outbursts (Maccarone 2003), and steep power law states are generally seen only at very high luminosities, near the Eddington limit (Remillard & McClintock 2006). This spectral state phenomenology allows, with high quality spectra, a source to be classified as a candidate BH XB on the basis of its having a cool accretion disk at 10^{38} erg s^{-1}, as discussed by White & Marshall (1984). Burke et al. (2012) used the Cen A VLP data to show that such distinctions are now possible for sources outside the Local Group, presenting evidence that CXOU J132527.6-430023 (S14, Table 1) is a BH LMXB.

The relative proximity of Cen A, coupled with the superb quality of these data, allows us unrivaled insight into the XBs of an early-type galaxy. In this work we divide sources into thermal and non-thermally dominant states, where appropriate, down to a luminosity of 2×10^{37} erg s^{-1} – reliably measuring the spectral properties of XBs at similar luminosities to those found in the Local Group.

2. DATA PREPARATION

2.1. *Source Detection and Alignment*

Each of the six 100 ks observations was analysed using CIAO 4.3, and was reprocessed using the *chandra_repro* script. The *destreak* tool was used to remove the ACIS read-out streak, caused by the bright Cen A nucleus. Light curves of each event file were produced using *dmextract* to check for background flares, which were not present. To search for point sources, we used a 0.5-2.0 keV event file for each observation. We used this band because the central AGN is so bright (6-10 count s^{-1} in ACIS-I) that the wings of the PSF contain a significant number of counts, the PSF being broader at higher energies for *Chandra*. An exposure map was created for each file, weighted by the typical power law spectrum of an LMXB, with a photon index of $\Gamma = 1.7$ and absorption column at the Galactic value of $N_H = 8.4 \times 10^{20}$ cm^{-2} (Dickey & Lockman 1990). Inside a $5'$ region centered on the Cen A nucleus, we located point sources using the CIAO tool *wavdetect* using the spectrally weighted exposure map, wavelet scales of 1.0 to 16.0 in steps of $\sqrt{2}$, a threshold significance of 10^{-6} and a maximum of ~ 1 false source per ACIS chip. All subsequent work is within $5'$ of the Cen A nucleus, which corresponds to $\sim$ the half-light radius of Cen A (Graham 1979).

The six observations were aligned by applying an appropriate x-y shift to five of the aspect solution files using the CIAO tool *reproject_events*. All observations were aligned to the point source positions from obsID 8490, chosen because of the proximity of the Cen A nucleus to the ACIS-I focus. Each shift was calculated from the mean offset in α and δ obtained

performing $2''$ matching between point source lists from the two observations. To reduce the effect of false matches on our offset correction, we found the mean offset in α and δ and then calcuated the mean offset within $\pm 0.5''$ of this mean. By applying $5''$ shifts in α and δ, subsequent $2''$ matching found ~ 6 false matches between source lists.

To allow for accurate analysis of globular cluster (GC) sources in our subsequent work, we utilized the well known LMXB-GC connection to align our observations to GC positions (Harris et al. 2012), again using $2''$ matching (we estimate an approximate GC size of $\sim 2''$), we calculated the mean x-y shift between LMXB positions in obsID 8490 and the globular clusters, and applied this shift to all obsID, maintaining the initial alignment of the X-ray data.

We created a merged event file using the CIAO script *merge_all* and a corresponding exposure map, as before. The point source list produced by a subsequent run of *wavdetect* was used as a master list of source positions that was consistent with the positions of the individual runs on each obsID, for each observation in which the source was detected. Circular extraction regions were produced, centered on the chip position of each source, whether it is detected in an observation or not. As was the case for the work of Burke et al. (2012), these regions had radius r_{p7}, equal to 90% of the 7 keV extraction radius at that chip position. We then excluded regions in the jet, radio lobe and nucleus from our source list. Additional region files were produced, covering the removed read-out streak of the bright central AGN. Background region files were then created based on annuli from $2r_{p7}$ to $4r_{p7}$, with all source regions and the read-out region excluded. Subsequently we tested for source confusion, which was a significant problem in observations 7798 and 7799, where the point source population is further off-axis and the point-spread function is much wider. Sources found to have a neighbor at angular half-distance $d/2$ inside r_{p7} were given a new extraction region radius of $d/2$ provided that $d/2 \geq r_{p2}$ (where r_{p2} is 90% PSF radius at 2keV), while sources with $d/2 < r_{p2}$ were declared confused (Table 1). Spectral fitting using various sized extraction regions for isolated, off-axis sources determined that the normalisation found from fitting was consistent between r_{p2} and r_{p7}, but increased systematically as the extraction radius decreased further.

The net counts inside each extraction region were estimated using *dmextract* to the requisite properties of the source and background region, followed by using *aprates* to calculate a 90% confidence bound for each value or, where appropriate, a 90% confidence upper-limit. Sources were then sorted, based on their highest count-flux observed in any individual observation and names assigned based on this ranking. We present these results in Table 1, and emphasize that these are *not* the estimated source counts, but the net source counts present in a given extraction region. This indicates the quality of the resulting spectra we extracted for a given source.

2.2. *Source Selection*

The presence of short-term variability may indicate important spectral changes within an X-ray source, and so we choose to exclude sources that vary during an observation from our sample. To assess the variability we made use of the Gregory-Loredo algorithm (Gregory & Loredo 1992), implemented as the CIAO tool *glvary*[17]. This produces an

---

[17] $http://cxc.harvard.edu/ciao/ahelp/glvary.html$

optimally-binned lightcurve for each source in each observation, and calculates an odds ratio of each lightcurve against a constant count-rate, with a ratio of 10 indicating the highest probability of variation and 0 being consistent with a constant count rate. A source is defined as showing definite variability when this index is ≥ 6. The maximum ratio for each source is reported in Table 1. Given the potential for rapidly changing spectra within an observation, sources with a maximum score of 6 or higher were removed from our sample for spectral analysis.

At this point we also flagged sources within $20''$ of the Cen A nucleus, which require more careful extraction to deal with the significant flux contribution present from the nucleus. This contribution likely exceeds the source counts in some observations for any sources with fewer than ~ 300 counts, depending on how far off-axis the nucleus is in the observation. Analysis of the sources that showed definite intra-observation variability and the sources within $20''$ of the nucleus will be reported in a future work.

Table 1 summarises some basic source data; the celestial position, net counts in each source region for each observation and the intra-observational variability ($G - L_{max}$). We also include our eventual source classification of persistent (P) or transient (T) black hole candidates (BHC), neutron star candidates (NSC), foreground stars (FG), active galactic nuclei (AGN) and also denote S48 as a highly-magnetised NSC (β).

The distribution of hardness ratios showed that source S50 was far softer than the rest of the population, with $S/H \sim 9$ where S is the counts from 0.5–2.0 keV and H is the counts from 2.0–8.0 keV. The spectrum of this source was well fit with an absorbed apec model (Raymond & Smith 1977), peaking at 0.9 keV, across all observations, consistent with expectations from a foreground star. Inspection of the data taken with the Inamori Magellan Areal Camera and Spectrograph (IMACS) camera on the Magellan Observatory Baade telescope (Harris et al. 2012), showed that S50 is coincident with an object consistent with being stellar. We used ishape, which determines an object's shape parameters by analytically convolving a *King62* (King 1962) model with the PSF of the image, which is then subtracted from the input image of the object itself. From the residual image, the pixels are assigned a weighting based on their deviation from other pixels at the same distance from the center of the object, and then a reduced χ^2 is calculated. The initial parameters of the model are adjusted and the process is repeated with the new model until a minimation of the χ^2 is obtained and convergence is reached. Our best fit with *ishape* indicates that our object has a FWHM of 0.02 pc, consistent with a star, and very different from the typical globular cluster which are generally 2-4 pc in size (Harris et al. 2010), and we do not consider it further.

TABLE 1
BASIC SOURCE PROPERTIES

Source	α	δ	Net Counts (0.5 – 8.0 keV)						$G-L_{max}$	Type	Notes
			7797	7798	7799	7800	8489	8490			
S1	$13^h25^m18.25^s$	$-43°03'04''.9$	7183^{279}_{139}	8366^{302}_{151}	7372^{284}_{142}	6623^{270}_{134}	9624^{323}_{161}	8454^{303}_{151}	5		Sivakoff et al. (2008)
S2	$13^h25^m38.29^s$	$-43°02'05''.6$	1685^{136}_{68}	1364^{122}_{61}	1429^{125}_{62}	1062^{108}_{54}	1858^{142}_{71}	1366^{122}_{61}	9		
S3	$13^h25^m02.70^s$	$-43°02'43''.3$	1120^{110}_{55}	FoV	FoV	917^{103}_{51}	1575^{132}_{66}	981^{103}_{52}	1	NSC	
S4	$13^h25^m26.16^s$	$-43°01'32''.6$	1101^{114}_{57}	929^{107}_{53}	897^{105}_{52}	555^{87}_{43}	197^{56}_{28}	29^{35}_{17}	0	TBHC	D
S5	$13^h25^m07.64^s$	$-43°01'15''.3$	880^{98}_{49}	174^{46}_{23} C	176^{46}_{23} C	726^{93}_{46}	1009^{105}_{53}	1040^{106}_{53}	5	NSC	GC0129
S6	$13^h25^m06.30^s$	$-43°02'21''.1$	741^{90}_{45}	FoV	FoV	614^{86}_{43}	1024^{105}_{53}	613^{82}_{41}	6		
S7	$13^h25^m23.69^s$	$-43°00'09''.5$	756^{91}_{46}	787^{96}_{48}	871^{101}_{50}	655^{87}_{44}	608^{82}_{41}	603^{82}_{41}	0	NSC	D
S8	$13^h25^m22.88^s$	$-43°01'24''.9$	818^{96}_{48}	703^{94}_{47}	557^{83}_{41}	829^{100}_{50}	618^{85}_{42}	651^{86}_{43}	0	NSC	
S9	$13^h25^m28.19^s$	$-43°00'56''.5$	539^{97}_{48}	684^{102}_{51}	701^{103}_{51}	747^{104}_{52}	431^{91}_{45}	368^{95}_{47}	0		N
S10	$13^h25^m27.45^s$	$-43°02'14''.1$	600^{83}_{41}	SC	SC	SC	537^{78}_{39}	451^{72}_{36}	8		
S11	$13^h25^m54.57^s$	$-42°59'25''.4$	408^{69}_{35}	278^{55}_{28} C	313^{58}_{29} C	353^{62}_{31}	402^{67}_{33}	533^{80}_{40}	0	NSC	GC0330
S12	$13^h25^m32.45^s$	$-43°01'34''.2$	483^{75}_{37}	496^{78}_{37}	440^{74}_{37}	289^{62}_{31}	448^{72}_{36}	291^{59}_{30}	1	PBHC	D
S13	$13^h25^m25.76^s$	$-43°00'55''.8$	451^{76}_{38}	445^{85}_{42}	419^{83}_{41}	208^{68}_{34}	159^{53}_{27}	418^{75}_{37}	0	TBHC	D
S14	$13^h25^m27.58^s$	$-43°00'23''.3$	407^{69}_{34}	409^{74}_{37}	421^{75}_{37}	292^{66}_{33}	19^{25}_{12}	1^{14}_{1}	0	TBHC	D, Burke et al. (2012)
S15	$13^h25^m26.43^s$	$-43°00'54''.2$	309^{68}_{34}	271^{66}_{33}	322^{70}_{35}	225^{64}_{32}	147^{55}_{28} R	417^{78}_{39}	0		N
S16	$13^h25^m31.59^s$	$-43°00'03''.0$	303^{59}_{29}	327^{63}_{31}	338^{64}_{32}	400^{68}_{34}	353^{63}_{31}	409^{70}_{35}	1	NSC	GC0225
S17	$13^h25^m12.89^s$	$-43°01'14''.6$	405^{67}_{33}	311^{63}_{31}	288^{61}_{30}	323^{64}_{32}	349^{63}_{31}	84^{31}_{15}	0	NSC	
S18	$13^h25^m27.50^s$	$-43°01'28''.1$	368^{76}_{38}	323^{81}_{40}	370^{83}_{42}	345^{83}_{41}	355^{74}_{37}	364^{75}_{37}	0		N
S19	$13^h25^m27.08^s$	$-43°01'59''.2$	335^{64}_{32}	274^{71}_{35}	317^{75}_{37}	194^{64}_{32}	363^{66}_{33}	280^{59}_{29}	0	NSC	
S20	$13^h25^m28.75^s$	$-42°59'48''.3$	287^{58}_{29}	301^{62}_{31}	341^{65}_{32}	332^{63}_{31}	329^{61}_{30}	256^{56}_{28}	0	NSC	
S21	$13^h25^m22.32^s$	$-42°57'17''.3$	282^{57}_{28}	172^{48}_{24}	330^{63}_{31}	244^{53}_{26}	286^{57}_{29}	312^{62}_{31}	10		
S22	$13^h25^m40.54^s$	$-43°01'14''.9$	265^{55}_{28}	258^{54}_{27}	312^{59}_{29}	217^{50}_{25}	112^{35}_{18}	307^{59}_{30}	1	NSC	
S23	$13^h25^m35.50^s$	$-42°59'35''.2$	186^{47}_{23}	271^{55}_{28}	280^{56}_{28}	308^{59}_{29}	295^{59}_{29}	256^{56}_{28}	6		GC0249
S24	$13^h25^m11.99^s$	$-43°00'10''.7$	288^{56}_{28}	270^{61}_{30}	256^{60}_{30}	256^{58}_{29}	259^{57}_{27}	129^{38}_{19}	1		D
S25	$13^h25^m09.56^s$	$-43°05'29''.2$	286^{57}_{29}	FoV	FoV	SC	65^{31}_{16}	53^{26}_{13}	1	NSC	
S26	$13^h25^m46.58^s$	$-42°57'03''.1$	264^{57}_{28}	247^{52}_{26}	284^{56}_{28}	272^{55}_{27}	92^{34}_{17}	226^{53}_{26}	2	NSC	GC0295
S27	$13^h25^m43.97^s$	$-43°06'06''.8$	273^{56}_{28}	211^{51}_{25}	248^{55}_{27}	70^{37}_{19}	202^{48}_{24}	206^{49}_{24}	6		
S28	$13^h25^m24.19^s$	$-42°59'59''.4$	269^{56}_{28}	SC	SC	226^{52}_{26}	271^{56}_{28}	213^{51}_{25}	0	PBHC	D
S29	$13^h25^m33.93^s$	$-42°58'59''.7$	217^{50}_{25}	217^{50}_{25}	232^{52}_{26}	215^{49}_{24}	257^{54}_{27}	224^{52}_{26}	0	NSC	
S30	$13^h25^m12.03^s$	$-43°00'44''.7$	254^{53}_{26}	SC	SC	R	228^{51}_{25}	81^{30}_{15}	6		
S31	$13^h25^m23.57^s$	$-43°02'20''.5$	246^{53}_{26}	209^{58}_{29}	161^{54}_{27}	219^{58}_{29}	215^{50}_{25}	242^{52}_{26}	0	NSC	
S32	$13^h25^m09.18^s$	$-42°58'59''.3$	249^{53}_{26}	214^{53}_{26}	177^{48}_{24}	209^{52}_{26}	207^{50}_{25}	123^{38}_{19}	0	NSC	GC0134
S33	$13^h25^m23.52^s$	$-43°01'38''.4$	227^{52}_{26}	SC	SC	SC	236^{52}_{26}	243^{53}_{26}	7		
S34	$13^h25^m33.34^s$	$-43°00'52''.7$	208^{51}_{26}	208^{54}_{27}	192^{52}_{26}	193^{52}_{26}	224^{51}_{26}	219^{53}_{27}	0	NSC	D
S35	$13^h25^m18.50^s$	$-43°01'16''.1$	49^{9}_{4}	SC	SC	SC	91^{18}_{8}	218^{50}_{25}	1	T-	GC0182
S36	$13^h25^m32.01^s$	$-43°02'31''.3$	217^{50}_{25}	207^{52}_{26}	212^{52}_{26}	188^{51}_{25}	84^{31}_{16}	153^{42}_{21}	2	NSC	
S37	$13^h25^m29.45^s$	$-43°01'08''.1$	162^{60}_{30}	90^{74}_{37}	146^{77}_{38}	19^{50}_{19}	213^{60}_{30}	153^{60}_{30}	0		N
S38	$13^h25^m22.85^s$	$-43°00'17''.4$	2^{10}_{2}	9^{24}_{9}	3^{19}_{3}	0^{15}_{0}	1^{9}_{1} R	194^{48}_{24}	0	BHC	D
S39	$13^h25^m28.42^s$	$-43°03'15''.2$	162^{43}_{21}	187^{50}_{25}	163^{47}_{24}	171^{49}_{25}	58^{26}_{13}	110^{35}_{18}	1	AGN	
S40	$13^h25^m26.95^s$	$-43°01'04''.8$	171^{66}_{33}	SC	SC	SC	133^{38}_{13}	186^{65}_{32}	0		N
S41	$13^h25^m26.94^s$	$-43°00'52''.5$	136^{56}_{28}	162^{57}_{29}	135^{55}_{27}	164^{60}_{30}	120^{54}_{30}	182^{62}_{31}	1		N
S42	$13^h25^m16.40^s$	$-43°02'55''.1$	190^{46}_{23}	133^{48}_{24}	137^{48}_{24}	137^{49}_{24}	163^{44}_{22}	103^{34}_{17}	0	NSC	
S43	$13^h25^m28.20^s$	$-43°02'53''.4$	156^{43}_{21}	108^{40}_{20}	112^{41}_{20}	98^{39}_{19}	179^{45}_{22}	170^{44}_{22}	6		
S44	$13^h25^m20.06^s$	$-43°03'10''.1$	166^{43}_{22}	94^{43}_{21}	134^{47}_{23}	124^{46}_{23}	146^{41}_{20}	136^{39}_{20}	2	NSC	GC0587
S45	$13^h25^m39.06^s$	$-42°56'53''.7$	78^{36}_{18}	104^{35}_{17}	51^{26}_{13}	158^{42}_{21}	87^{33}_{17}	125^{45}_{23}	2	NSC	
S46	$13^h25^m25.15^s$	$-43°01'26''.9$	146^{49}_{24}	SC	SC	SC	125^{46}_{23}	88^{41}_{21}	0	NSC	D
S47	$13^h25^m23.07^s$	$-43°01'45''.6$	139^{43}_{21}	SC	SC	SC	128^{42}_{21}	147^{44}_{22}	2	NSC	
S48	$13^h25^m32.42^s$	$-42°58'50''.2$	87^{34}_{17}	143^{42}_{21}	104^{36}_{18}	133^{39}_{19}	87^{32}_{16}	121^{41}_{20}	1	β NSC	GC0230
S49	$13^h25^m52.72^s$	$-43°05'46''.4$	72^{33}_{17}	61^{30}_{15}	108^{37}_{19}	108^{40}_{20}	71^{31}_{15}	138^{42}_{21}	9		GC0320
S50	$13^h25^m10.09^s$	$-42°56'08''.3$	FoV	FoV	FoV	138^{45}_{22}	124^{43}_{21}	75^{37}_{18}	0	FG	
S51	$13^h25^m45.47^s$	$-42°58'15''.8$	117^{40}_{20}	114^{36}_{18}	118^{36}_{18}	123^{37}_{19}	133^{40}_{20}	95^{40}_{20}	6		
S52	$13^h25^m25.50^s$	$-43°01'29''.9$	127^{48}_{24}	SC	SC	SC	0^{NA}_{NA}	8^{22}_{8}	0		N
S53	$13^h25^m23.50^s$	$-42°56'51''.7$	111^{37}_{18}	119^{41}_{20}	131^{42}_{21}	113^{37}_{18}	95^{36}_{18}	129^{44}_{22}	1	NSC	
S54	$13^h25^m23.63^s$	$-43°03'25''.7$	58^{26}_{13}	58^{35}_{18}	66^{37}_{18}	82^{40}_{20}	117^{37}_{18}	25^{17}_{8}	1		
S55	$13^h25^m39.87^s$	$-43°05'01''.8$	110^{36}_{18}	111^{38}_{19}	103^{37}_{18}	97^{39}_{19}	92^{32}_{16}	87^{32}_{16}	0	NSC	GC0266
S56	$13^h25^m38.10^s$	$-43°05'13''.7$	62^{27}_{14}	71^{32}_{16}	80^{33}_{16}	74^{36}_{18}	81^{31}_{16}	112^{36}_{18}	0		
S57	$13^h25^m55.11^s$	$-43°01'18''.3$	96^{37}_{18}	96^{33}_{16}	77^{30}_{15}	84^{31}_{16}	91^{33}_{16}	112^{41}_{22}	0		
S58	$13^h25^m24.76^s$	$-43°01'24''.6$	22^{31}_{15} R	R	R	SC	77^{39}_{20}	112^{43}_{22}	0		
S59	$13^h25^m07.71^s$	$-42°56'29''.8$	FoV	FoV	FoV	66^{35}_{18}	103^{41}_{20}	109^{40}_{20}	2	NSC	
S60	$13^h25^m23.07^s$	$-43°01'34''.3$	103^{39}_{19} R	SC	SC	SC	100^{39}_{19}	80^{36}_{18}	0		
S61	$13^h25^m11.55^s$	$-43°02'26''.3$	103^{34}_{17}	SC	SC	SC	78^{31}_{15}	109^{35}_{17}	6		

NOTE. — Type column is explained in section 2.2, see also the extended discussion in section 4. N: Within $20''$ of the Cen A nucleus, R: Source is coincident with read-out streak, C: Source is coincident with chip-edge, FoV: Source is outside of the field-of-view, SC: Source confused, GC: Coincident with globular cluster, D: Coincident with dust lane

3. SPECTRAL ANALYSIS

Our primary objective is using spectral fitting of sample models to infer the spectral state of each source. Ideally, this would involve fitting all observations of a given source together, taking advantage of more bins to reduce the high-likelihood region of the parameter space. A more constrained absorption parameter, N_H provides a stronger argument for a given spectral state (see section 3.2). However, it is often the case with joint fitting that spectra from different states of a source will produce a best fit that, while well constrained and even statistically 'acceptable', may poorly represent the true spectra individually. To address this issue, we designed a comparative test between the spectra to allow us to judge the extent of spectral changes for each source, and thus the appropriateness of joint fits. Since we allow for changes in luminosity for a given spectral state, and only sought to determine a difference in the spectral shape of a source, the normalization of each spectrum is kept free in the joint fits.

Spectra were extracted using the CIAO script *specextract* for each observation that had > 100 net counts. We chose to fit only spectra where we had either > 150 counts in one observation, or more than two observations with > 100 counts.

3.1. *Spectral Variation*

Using the spectral fitting package *XSPEC* (Arnaud 1996), we performed spectral fits using an absorbed power law to the ungrouped spectrum, then used the covariance matrix of each fit in a subsequent Markov chain Monte Carlo (MCMC) exploration of the parameter space for each spectrum of each source in the sample.

7798–8489
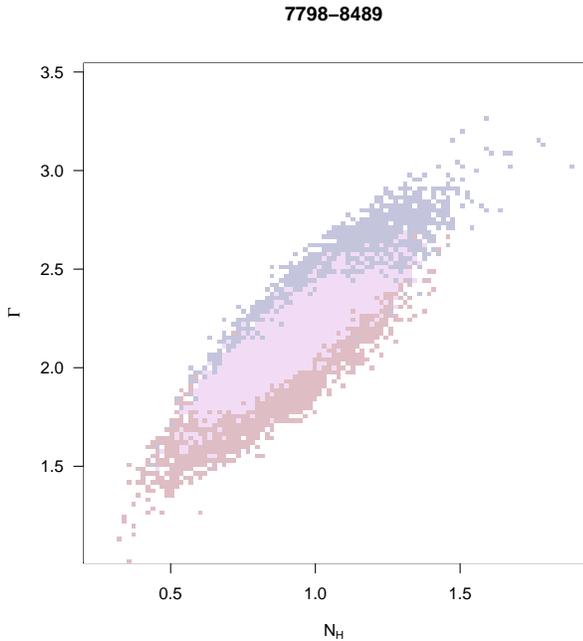
FIG. 1.— Example MCMC output binned over N_H and Γ for two spectra of S24. We show 90% confidence regions, with the overlap indicated by the lighter region. There is an $\sim$ 75% probability that true combinations of N_H and Γ are shared between the two MCMCs.

We then tried to compare each spectrum with the (up to) five other spectra for a given source. For the MCMC results

of a particular spectrum, we binned the parameter values of N_H and Γ, which describe the spectrum, into a 100×100 grid; the resulting bin widths were used to extend the grid, if necessary, to cover the other set of parameter co-ordinates. This approach was intended to prevent the binning being too coarse or fine, the extent of the MCMC-explored region of the parameter space increasing as the number of counts in a given spectrum decreased. The number of counts in each bin, normalized by the total number of samples, gives the approximate 2D posterior probability density for the $N_H - \Gamma$ space. The probability that the true coordinate is in an overlapping bin is the product of the sum of the probabilities for all the overlapping bins from both distributions. We adopted an a priori threshold of < 5% for determining if two spectra were too dissimilar to use in a joint fit, and the resulting spectral groups can be seen in our preliminary spectral fitting results (Table 3). We show typical 90% confidence interval contours (fewest bins to contain 90% of all samples) of two similar spectra from S24 in figure 1. For a handful ($\sim$ 3) of instances when the behaviour of a source was not clear cut, i.e. spectrum *A* and spectrum *B* were different, while both were consistent (> 5%) with spectrum *C* we took the more consistent of the two groupings, guided by the 90% confidence contours (i.e. a noticeable difference in shape inside the parameter space between two groups).

3.2. *Spectral Fitting*

After identifying sets of spectra for each source, we proceeded to fit absorbed single-component models to the 0.5-8.0 keV spectra, following the prescription of Brassington et al. (2010), who showed that the results from such fits – particularly the behavior of absorption parameter N_H – can give a strong indication of the actual spectral state of a given source. These results are summarised as a scheme for spectral fitting by means of a flow-chart in Figure 16 of Brassington et al. (2010), and we direct the interested reader to inspect this chart in tandem with our results. For thermally dominant spectra, where a disk blackbody component accounts for > 60% of the source flux, show a level of absorption significantly above the Galactic value N_H^{Gal} (Dickey & Lockman 1990) when fit with an absorbed power law, while a power law dominated spectrum will have an absorption less than the Galactic value when fit with an absorbed disk blackbody. If N_H is significantly above the Galactic value for both fits, then the source was deemed to have intrinsic absorption. If N_H was above N_H^{Gal} for the power law fit but significantly below N_H^{Gal} for the *diskbb* model, then this indicates a thermal dominant spectrum with some power law component also present. Conversely, if N_H from fitting was zero for both models, then this was indicative of the source spectrum being dominated by a steep ($\Gamma > 1.7$) power law component with a cool ($kT_{in} < 0.5$ keV) disc component also present. More specific effects are discussed in section 4.

We present results of fitting *phabs $\times$ powerlaw* and *phabs $\times$ diskbb* in Table 3, and indicate in the last column the spectral state(s) suggested by the Brassington et al. (2010) systematic scheme. We emphasize that the results in this table demonstrate a phenomenological test. Sources judged to be in a thermal dominant or power law dominant state were subsequently re-fit, imposing a lower limit on N_H at N_H^{Gal}, and we refer the reader to Table 2 for the realistic source properties. The tendency for so many of the sources coincident with the dust lane to have an inferred 'intrinsic' absorption (i.e., N_H

from both absorbed power law and disk blackbody models was significantly above N_H^{Gal}), meant that we tried to determine the 'true' absorbing column along those lines-of-sight, for a more realistic and useful comparison.

3.3. *Dust lane sources*

There is clearly a strong correlation between sources that possess intrinsic absorption, according to our method, and coincidence with the dust lane, as expected if the sources lie behind or within the dust. To define the spectral states for these sources, we obtain a value of N_H independently from the X-ray spectral fitting, and consider the extra absorbing column in Cen A as well as the Galactic contribution. We converted a K-band optical depth map of the dust lane (Kainulainen et al. 2009) to N_H assuming $A_K \sim 0.09 A_v$ (Whittet 1992) and $N_H \sim A_v \times 2.1 \times 10^{21}$ cm^{-2} (Güver & Özel 2009). The mean N_H was then calculated using the IRAF tool *imexam*[18] for each source coincident with the dust lanes, using circular apertures of radius $2''$, centered on the source position. The N_H^{DBB} and N_H^{PO} from spectral fitting were compared to the mean N_H inferred from the optical depth map at each source position, to infer the true spectral state, if possible. Dust lane sources that we determined to be dominated by disk blackbody or power law spectra are included in Table 2, and in Figures 2 & 3 when the parameters could be constrained. A full discussion of these sources can be found in Section 4.1.

3.4. *Inter-Observation Variability*

We can further our knowledge of these sources by taking the degree of inter-observational variability into account over the course of our 2 month snapshot. We calculated the net photon flux[19] for each source region using the ciao tool *aprates*[20], after calculating the average effective exposure in the region using a 0.5-8.0 keV exposure map. To assess the variability, we calculate the fractional variability of the source, which we define for a set of fluxes F_i as $(F_{max} - F_{min})/F_{max}$. For sources that are below the detection threshold in some observations, the 90% upper-limit was used for F_{min}. We present these resuls in Figure 4, where we show the fractional variability against spectral parameter (kT_{in} & Γ) for a given spectral state. The majority of sources display $10-40\%$ variability over the time period spanned by the VLP.

4. DISCUSSION

In this section we first discuss each source coincident with the dust lane in turn, identifying the spectral state our method favors where possible. We then present the unabsorbed luminosities as a function of key parameters of thermal and power law dominated states, and discuss the implications and source classification based on these results. We discuss possible transient NS LMXBs in outburst and also those states for which we are not able to make an adequate diagnosis using simple models. Finally, we offer an explanation for an apparent enhancement in the number of accreting BHCs found beyond the vicinity of the merged late-type galaxy.

4.1. *Dust lane sources*

For those sources that are coincident with the dust lane and where spectral fitting suggests a high N_H we infer the spec-

[18] http://stsdas.stsci.edu/cgi-bin/gethelp.cgi?imexamine
[19] We emphasise that this does not involve assuming a spectral model
[20] http://cxc.harvard.edu/ciao4.2/ahelp/aprates.html

tral state of a given source based on the mean absorption calculated from a K-band optical depth map. Due to the extra level of consideration given to the dust lane sources, we discuss each source in turn below, and where a particular state is suggested we present it in Table 2. Our spectral diagnostic, inferring the state from fitting simple spectral models, is outlined in section 3.2.

4.1.1. *S4*

The brightest dust lane source, S4, is $\sim 30''$ from the Cen A nucleus, coincident with a southern filament of the dust. From the optical depth map we calculate $N_H = (3.64 \pm 0.07) \times 10^{21}$ cm^{-2}, which, while above the Galactic value, is still below $N_H^{DBB}(= 6.5 \times 10^{21}$ cm$^{-2})$. It seems likely that the spectrum is dominated by a thermal component; the discrepancy in absorption is either a consequence of additional intrinsic absorption from material local to the source, or the result of some significant non-thermal component contributing to the spectrum. The true kT_{in} may be somewhat cooler than that found from just fitting *phabs*(*diskbb*), as suggested by the simulations of Brassington et al. (2010), an effect we discuss in more detail for S12. Fixing N_H at the value obtained from the optical depth map preserves the cool disk temperature in spectral fitting. There is a large fall in flux from this source, the spectral counts falling to 29 in the final observation from over 1100 in the first; however, it is still above our detection limit. The low inner-disk temperature in the thermal state, combined with the high inter-observation variability, strongly suggests that this is a BH LMXB transient candidate, similar to S14 (Burke et al. 2012). NS LMXBs at this luminosity, $L_x > 10^{38}$ erg s^{-1}, typically have a much flatter spectral shape over the *Chandra* band.

4.1.2. *S7*

For S7 the absorption map gave $N_H = (6.52 \pm 0.08) \times 10^{21}$ cm^{-2}, which is below N_H^{PO} but above N_H^{DBB}. This suggests that the source is behind the dust lane in a thermal dominant state, but with some power law component present. We are not able to determine the flux contribution of the power law component. Based on the simulations of Brassington et al. (2010) we estimate the absolute systematic error ± 0.5 keV on the temperature of the disk component.

4.1.3. *S12*

In the case of S12, the inferred $N_H = (16.5 \pm 0.2) \times 10^{21}$ cm^{-2}. This is significantly above the values found from spectral fitting, and allows for the source to be located within the dust lane, rather than behind it. If we assume that the source is behind the dust lane, i.e. has a line-of-sight absorption column of $N_H = (16.5 \pm 0.2) \times 10^{21}$ cm^{-2}, then we have fitting results that were not produced by the simulation work of Brassington et al. (2010), where N_H^{DBB} went to zero and N_H^{PO} was less than the Galactic value, which was the result obtained when the simulated spectrum was a dominant, steep power law component with a cool disk also present. Those simulations were based on a fairly low value of N_H, less than 1×10^{21} cm^{-2}, and so the tendency for N_H^{DBB} to go to zero for instances where $N_H^{PO} < N_H^{Galactic}$ is not surprising, as N_H^{DBB} will nearly always be less than N_H^{PO} and so the size of the high-likelihood region of the parameter space is small.

To investigate our ability to recover the parameters of a heavily absorbed cool disk plus steep power law spectrum,

we carried out simulations in XSPEC. We assumed a heavily absorbed ($N_H \sim 1.6 \times 10^{22}$ cm^{-2}) cool disk ($kT_{in} \sim 0.4$ keV) and a steep power law ($\Gamma \sim 2.6$). Sets of 200 simulated spectra were produced, varying the *diskbb* fraction of the total flux from 0.1 to 0.9. We then fitted *phabs* $\times$ *diskbb* to these spectra to look at the effect of varying the initial spectral parameters on those recovered by fitting a simple, single component spectrum. We found that the fits recovered the initial properties of the disk when the simulated spectrum was thermally dominated, but as the fraction of flux taken by the power law component increased in significance, so the recovered value of N_H decreased, eventually reaching N_H^{DBB} comparable with that found from fitting the spectra of S12. A consequence of lower N_H^{DBB} as the power law contribution increased was that the recovered inner-disk temperature rose to beyond 1.5 keV. This fits neatly with the *phabs* $\times$ *diskbb* fit to S12, which has a high value of kT_{in} (=$3.96^{-1.73}_{+0.87}$ keV), implying an unphysically massive stellar BH. We take this result as an indication that our assumption about S12 is correct; that it is obscured fully behind the dust lane, with a line-of-sight $N_H > 10^{22}$ cm^{-2}, and has a spectrum dominated by a power law with some small disk contribution. Further simulations suggest that high inner-disk temperatures (> 3 keV) are also recovered with a less steep power law component ($\Gamma < 1.5$). This is clearly a complicated parameter space, the full properties of which are beyond the scope of this work to investigate. It is worth noting that these results indicate a significant under-estimation in the flux of the source by just fitting simple models; the actual L_x is probably $> 6 \times 10^{38}$ erg s^{-1}, and could conceivably $> 10^{39}$ erg s^{-1}, based on our simulations. Fitting more complex (two component) models failed to give acceptable fits or successfully accommodate both components, with poorly constrained parameters.

S12 is analogous to S102 in NGC 3379 (Brassington et al. 2010), for which simulations indicated that the spectra were dominated by a steep power law with some contribution from a cool disk, while a successful fit was achieved using a combined *diskbb* + *powerlaw* model yielding $kT_{in} \sim 0.14$ and $\Gamma \sim 1.6$ and $L_x = 1.1 \times 10^{39}$ erg s^{-1}.

4.1.4. *S13*

We calculate $N_H = (7.95 \pm 0.13) \times 10^{21}$ cm^{-2} in the vicinity of S13, which is below or consistent with the N_H^{PO} values obtained, but these are poorly constrained and the fits are statistically poor with $\chi^2_\nu > 1.3$. Conversely, N_H is above N_H^{DBB}, which is significantly larger than N_H^{Gal}. As was the case with S7, such results are indicative of a thermally dominant state with some non-thermal emission also present, by which we mean that the thermal state contributes $> 60\%$ of the total flux. The inner temperature in the disk of this source is less than that typically seen for NS systems at equivalent luminosities. This source displays high inter-observation variability, but remains in outburst throughout the length of our observations. This variability coupled with the low inner-disk temperature suggests that this system is a BHC LMXB, though examination of further observations will be required to show more substantive evidence of the transient nature of this source.

4.1.5. *S14*

S14 is a transient source, analysis of which has previously been reported in Burke et al. (2012). N_H^{PO} was larger than the value inferred from the dust lane, N_H^{DBB} was found to be consistent with this value, which led us to conclude the source

was in a thermally dominant state. The cool disk at high luminosity, coupled with its transient nature, led us to conclude that the source is a BH LMXB candidate. Our fitting results for the first group suggests the presence of a power law component in the more luminous state.

4.1.6. *S24*

While S24 is coincident with the dust lanes, its position is not covered by our optical depth map. This being the case we cannot feasibly proceed further with our inference of spectral states based on the behavior of N_H, given that our first stage of spectral fitting is highly suggestive of increased line-of-sight absorption, above the Galactic value.

4.1.7. *S28*

For S28, we find $N_H = (7.63 \pm 0.12) \times 10^{21}$ cm^{-2} from the K-band optical depth map. We fit two groups of spectra for this source. For the first group, consisting of spectra from obsIDs 7797 and 8490, we find a large uncertainty on N_H for both models, which is consistent with any location relative to the dust lanes at the 2σ level. The second group, using spectra from obsIDs 7800 and 8489, have N_H significantly above $N_H^{Galactic}$, which indicates that there is significant absorption along the line-of-sight to the source, which we attribute to the dust lane. For this group, N_H^{PO} is above the value obtained from the optical depth maps, while N_H^{DBB} is consistent with this value, suggesting that the source is in a thermally dominant state. Assuming that the source is behind the dust lane, as the second set of spectral fitting results suggests, and assuming a 1σ knowledge of $N_H^{PO} = 0.51^{0.26}_{0.24} \times 10^{22}$ cm^{-2} and $N_H^{DBB} = 0.44^{0.18}_{0.15} \times 10^{22}$ cm^{-2}, then, for the first group, the situation is similar to that seen in S12, where N_H^{PO} is consistent with the line-of-sight value while N_H^{DBB} is lower but non-zero. The higher, unrealistic (and poorly constrained), inner-disk temperature of 5.97 keV is consistent with this result, suggesting that the source is in a power law state during these epochs, with a minor contribution from a cool ($kT_{in} < 0.5$ keV) disk component.

4.1.8. *S34*

S34 is close to the edge of the dust lane but is not coincident with the lane itself. The high N_H in one of the spectral fitting groups, of which obsID 8490 provided the only spectrum, prompted us to investigate the line-of-sight absorption using the optical depth map; we found $N_H = (1.10 \pm 0.08) \times 10^{21}$ cm^{-2}, consistent with the Galactic value. We are not able to deduce more about the state from this information; the source could have some intrinsic absorption not present in the other obsIDs. This behavior is reminiscent of the black hole in globular cluster RZ 2109 from NGC 4472, where the variation in N_H is believed to be the result of a photoionizing, high-velocity wind (Shih et al. 2010). However, S34 is much fainter than this class of system, and the apparent increase in absorption could be an effect of incorrectly modelling the boundary layer emission, or the absorption may be a real effect and the system is at a high inclination, undergoing a long period of dipping.

4.1.9. *S38*

S38 is only detected in obsID 8490. From the optical depth map, we infer $N_H = (4.54 \pm 0.07) \times 10^{21}$ cm^{-2} for this source. This is consistent with N_H^{DBB} and significantly less than N_H^{PO},

suggesting a source in the thermally dominant state with an inner disk temperature ~ 0.65 keV, similar to S14, albeit at a lower luminosity of $L_x \sim 5.5 \times 10^{37}$ erg s^{-1}, which points to it being a transient BH LMXB candidate.

4.1.10. *S46*

The X-rays from S46 would only experience an absorption column of $N_H = (2.81 \pm 0.08) \times 10^{21}$ cm^{-2} if the source is behind the dust lane. N_H^{PO} is less than this line-of-sight value, and consistent with $N_H^{Galactic}$ while N_H^{DBB} tends to zero, suggesting a source in front of the dust lane, in a power law dominated hard state.

4.2. *BH & NS LMXBs*

None of the sources in our sample is confirmed to have $L_x > 4 \times 10^{38}$ erg s^{-1}, compared to 3 sources apiece in NGC 3379 and NGC 4278 in the sample of Fabbiano et al. (2010). We caution that our sample is drawn from within the half-light radius, as opposed to D_{25}, on account of the relative proximity of Cen A. In addition, Cen A is a slightly smaller galaxy with $M_B = -21.1$ (Ferrarese et al. 2007) compared to -22.28 and -22.02 for NGC 3379 and NGC 4278 (Cappellari et al. 2006), and the LMXB population scales with galaxy mass to first order. While we also exclude the sources that vary during the course of an observation or are close to the Cen A nucleus for a later study, it is unlikely that these sources have $L_x > 5 \times 10^{38}$ erg s^{-1} (Table 1) unless the intra-observation variability is extreme. Assuming the XLF follows an unbroken power law, with $dN/dL \sim KL^{\alpha}$ and $\alpha = -2$ (Kim & Fabbiano 2004), and assuming there are ~ 40 sources between $\sim 2 \times 10^{37}$ erg s^{-1} and $\sim 10^{38}$ erg s^{-1} (Table 1), then $K \sim 10^{39}$ and there would be ~ 8 sources between 10^{38} erg s^{-1} and 5×10^{38} erg s^{-1} and we would expect a single source in 5×10^{38} erg s^{-1} to 10^{39} erg s^{-1}. These values are consistent with our results.

We present the thermally dominant and power law dominant spectral properties in Figures 2 & 3, respectively. In Figure 2, we plot the unabsorbed disk luminosity against inner-disk temperature for the thermally dominant states (note that one point is representative of one ACIS spectrum, as we allowed for normalization, i.e. the flux, to be a free parameter during fitting), and we show illustrative bands of constant mass for $10M_\odot$, $5M_\odot$ and $2M_\odot$ assuming a non-rotating compact object (Gierliński & Done 2004), the width of the bands shows the variation with inclination θ, from $\cos\theta = 0.25$ to $\cos\theta = 0.75$ (for which we use correction factors presented in Zhang et al. 1997), and we assume $f_{col} = 1.8$. What is most striking is the apparent bimodal nature of the thermal state sources, between those that are consistent with, or to the right of our $2M_\odot$ band, and those to the left of the $5M_\odot$ b. In Figure 6 of Burke et al. (2012), we presented a population of Local Group thermal states, all of which lie to the left of our supposed $2M_\odot$ line. The fact that the bulk of our sources lie to the right of this line, with $kT_{in} > 1$ keV in the range of $L_x \sim 10^{37} - 10^{38}$ erg s^{-1}, is very suggestive that our thermal state sample is dominated by NS LMXBs.

We suggest tentatively that this result is reminiscent of the well-known 'mass gap' problem (Bailyn et al. 1998). The mass distribution of compact objects in transient systems strongly deviates from theoretical predictions, with a characteristic paucity between the most massive NSs ($\sim 3M_\odot$) and the least massive BHs, while the mass distribution of BHs is seen to peak at $\sim 8M_\odot$. If not a systematic effect

Source	N_H 10^{22} cm^{-2}	kT_{in} keV	L_x (0.5 - 10.0 keV) 10^{37} erg s^{-1}	χ^2/dof	Note
DBB					
S3	$0.08^{0.02}_{0.08}$	$1.82^{0.14}_{0.13}$	$24.58^{1.75}_{1.72}, 39.27^{2.41}_{2.36}$	120.7/140	
S4	$0.65^{0.07}_{0.06}$	$0.64^{0.03}_{0.03}$	$21.06^{2.23}_{2.04}, 37.49^{3.41}_{3.09}$	206.9/203	D
S4	$0.59^{0.48}_{0.35}$	$0.40^{0.13}_{0.11}$	$6.15^{7.79}_{2.57}$	10.0/14	D
S7	$0.51^{0.07}_{0.06}$	$1.49^{0.11}_{0.1}$	$18.6^{1.5}_{1.4}, 27.2^{1.8}_{1.8}$	271.5/256	D
S8	$0.08^{0.05}_{0.05}$	$1.93^{0.25}_{0.17}$	$15.71^{1.41}_{1.34}, 21.91^{1.85}_{1.76}$	135.7/132	
S8	$0.08^{0.03}_{0.08}$	$1.1.74^{0.3}_{0.23}$	$14.19^{1.37}_{1.29}, 21.07^{2.12}_{1.96}$	87.8/87	
S13	$0.40^{0.13}_{0.12}$	$0.83^{0.1}_{0.09}$	$10.57^{1.53}_{1.33}, 14.41^{1.93}_{1.69}$	110.7/89	D
S13	$0.39^{0.37}_{0.29}$	$0.56^{0.13}_{0.14}$	$4.34^{2.55}_{1.26}, 6.33^{3.72}_{1.77}$	37.5/30	D
S13	$0.35^{0.21}_{0.17}$	$0.71^{0.13}_{0.11}$	$11.65^{2.68}_{1.97}$	44.9/33	D
S14	$0.37^{0.12}_{0.11}$	$0.61^{0.07}_{0.06}$	$7.00^{1.24}_{1.03}, 12.33^{2.07}_{1.68}$	72.0/71	D
S14	$0.81^{0.28}_{0.23}$	$0.52^{0.08}_{0.08}$	$18.8^{7.4}_{4.4}$	14.6/27	D
S19	$0.09^{0.08}_{0.09}$	$1.50^{0.13}_{0.17}$	$5.45^{0.92}_{0.89}, 7.59^{0.85}_{0.8}$	119.3/135	
S22	$0.08^{0.03}_{0.08}$	$1.47^{0.11}_{0.14}$	$4.93^{0.71}_{0.68}, 6.49^{0.76}_{0.73}$	63.6/67	
S26	$0.08^{0.05}_{0.08}$	$1.70^{0.24}_{0.19}$	$6.13^{0.83}_{0.77}, 7.02^{0.97}_{0.89}$	51.6/60	GC
S28	$1.10^{0.45}_{0.4}$	$2.09^{0.97}_{0.5}$	$11.62^{1.76}_{1.66}, 11.9^{1.7}_{1.1}$	34.8/28	D
S31	$0.08^{0.05}_{0.08}$	$1.08^{0.15}_{0.13}$	$4.01^{0.57}_{0.53}, 4.20^{0.55}_{0.53}$	39.7/43	
S31	$0.12^{0.38}_{0.12}$	$0.98^{0.27}_{0.31}$	$3.1^{0.94}_{0.64}$	13.3/12	
S32	$0.08^{0.07}_{0.08}$	$1.66^{0.27}_{0.23}$	$5.26^{0.9}_{0.82}, 6.56^{1.08}_{0.98}$	28.2/50	GC
S32	$0.08^{0.13}_{0.08}$	$1.65^{0.55}_{0.34}$	$5.46^{1.19}_{0.97}, 7.67^{2.04}_{1.62}$	16.0/16	GC
S34	$0.08^{0.12}_{0.08}$	$1.99^{0.37}_{0.37}$	$4.71^{0.82}_{0.76}, 6.19^{1.01}_{0.92}$	52.6/67	
S38	$0.60^{0.52}_{0.43}$	$0.65^{0.25}_{0.17}$	$5.48^{3.68}_{1.70}$	7.8/9	D
S44	$0.08^{0.08}_{0.08}$	$1.21^{0.17}_{0.15}$	$2.41^{0.42}_{0.4}, 2.93^{0.48}_{0.45}$	29.3/42	GC
S45	$0.18^{0.26}_{0.18}$	$1.65^{0.63}_{0.41}$	$2.86^{0.65}_{0.6}, 3.65^{0.78}_{0.7}$	28.5/21	
PO		Γ			
S3	$0.13^{0.08}_{0.13}$	$1.25^{0.13}_{0.11}$	$36.29^{2.35}_{2.3}, 38.22^{2.74}_{2.65}$	109.6/117	
S5	$0.11^{0.05}_{0.11}$	$1.19^{0.09}_{0.08}$	$29.37^{1.91}_{1.87}, 36.56^{2.3}_{2.25}$	180/214	GC
S8	$0.08^{0.16}_{0.06}$	$1.31^{0.28}_{0.2}$	$21.11^{2.52}_{2.37}$	23.2/34	
S11	$0.08^{0.17}_{0.08}$	$1.29^{0.29}_{0.17}$	$13.52^{1.87}_{1.75}$	17.3/23	GC
S11	$0.09^{0.11}_{0.09}$	$1.54^{0.19}_{0.08}$	$12.44^{1.37}_{1.17}, 16.6^{1.54}_{1.36}$	72.3/73	GC
S16	$0.14^{0.08}_{0.14}$	$1.59^{0.15}_{0.14}$	$10.05^{1.09}_{1.06}, 14.26^{1.62}_{1.58}$	126.5/129	GC
S17	$0.16^{0.11}_{0.16}$	$1.45^{0.17}_{0.16}$	$10.77^{1.16}_{1.13}, 13.39^{3.07}_{3}$	93.1/105	
S20	$0.17^{0.10}_{0.17}$	$1.74^{0.18}_{0.17}$	$8.43^{0.98}_{0.95}, 11.25^{1.3}_{1.24}$	83.5/113	
S22	$0.08^{0.14}_{0.08}$	$1.98^{0.35}_{0.23}$	$5.85^{0.86}_{0.75}$	13.4/14	
S25	$0.11^{0.21}_{0.11}$	$2.11^{0.47}_{0.21}$	$6.24^{1.66}_{0.73}$	14/15	
S29	$0.16^{0.12}_{0.16}$	$1.85^{0.24}_{0.21}$	$5.86^{0.81}_{0.76}, 6.65^{0.87}_{0.82}$	65.1/64	
S36	$0.20^{0.23}_{0.2}$	$2.39^{0.61}_{0.41}$	$4.96^{2.11}_{1.03}, 5.08^{2.11}_{1.03}$	23.8/23	
S42	$0.13^{0.22}_{0.13}$	$1.69^{0.36}_{0.30}$	$3.97^{0.87}_{0.79}, 5.06^{1.06}_{0.99}$	46.5/44	
S46	$0.11^{0.45}_{0.11}$	$1.61^{0.61}_{0.21}$	$3.00^{0.99}_{0.77}, 4.28^{1.25}_{0.83}$	28.2/27	D
S47	$0.11^{0.26}_{0.11}$	$1.86^{0.53}_{0.2}$	$3.26^{0.82}_{0.6}, 3.52^{0.79}_{0.65}$	14.7/23	
S53	$0.30^{0.32}_{0.30}$	$2.29^{0.57}_{0.46}$	$3.25^{1.66}_{0.86}, 3.91^{1.81}_{0.93}$	16/19	
S55	$0.19^{0.59}_{0.19}$	$1.72^{0.83}_{0.31}$	$3.34^{1.56}_{0.73}, 4.36^{2.05}_{0.99}$	15.1/14	GC
S59	$0.11^{0.42}_{0.11}$	$1.57^{0.67}_{0.26}$	$2.91^{0.74}_{0.67}, 3.14^{0.91}_{0.67}$	9.8/12	

NOTE. — Spectral fitting results with the appropriate simple model for thermally dominant (**DBB**) and power law dominant (**PO**) states, with N_H forced to be above the Galactic value to reach a better estimate of the source luminosity. GC denotes that the source is coincident with globular cluster while D indicates that a source is in the vicinity of the dust lane.

(e.g. Farr et al. 2011; Kreidberg et al. 2012), then this feature in the mass distribution favours 'rapid' initial stellar collapse models of supernovae, where initial instabilities grow on timescales of 10-20 ms (Belczynski et al. 2012), over models that require more prolonged instability growth (> 200 ms). To quantitatively test if these data are distributed bimodally in this plane, we first calculate a 'mass' for each source based on the observed peak luminosity, assuming $\cos\theta = 0.5$. We then fitted[21] both a single Gaussian, and then dual Gaussians to the observed mass distribution and from these fits calculate the Akaike's Information Criterion (AIC) (Akaike 1974) for both models. The dual Gaussian fit had means (standard deviations) of 1.93 (0.76) $M_\odot$ and 15.74 (8.46) $M_\odot$ while the single Gaussian was centred on 5.6 (7.55) $M_\odot$. The AIC for the single Gaussian fit (=114.11) was larger than that of the dual Gaussian fit (=83.66), such that the latter was strongly favoured, with the single Gaussian 2.44×10^{-7} times as probable as the double Gaussian. These results are the first hint that the mass gap exists outside the Local Group.

BH systems do not have thermal emission from a boundary layer, as one would expect from the NS LMXBs. The flatness of the S3 and S5 spectra, which our method suggests are power law dominated with $\Gamma \sim 1.2$, is more consistent with the spectra of LMXB NS Z-track sources than those of BH sources in the hard state at $L_x > 10^{38}$ erg s^{-1}. We know this based on simulating the spectra of NS LMXBs using the model and parameters reported by Lin et al. (2012), who modeled the spectra of a bright NS LMXB, GX17+2, using a combination of disk blackbody, blackbody, and a power law component that is significant only on the Z-track horizontal branch. Regardless of whether this is a physically correct description or not, it is clearly a good phenomenological description of the spectral shape. At similar count rates to S3 and S5, we find that the parameters of this multi-component model are poorly recovered by a two-component $phabs(diskbb+bbody)$ fit, but that the shape of the spectrum is typically well-described by a shallow power law of $\Gamma \sim 1.0-1.4$, which does not vary substantially between Z-track states over the *Chandra* bandpass. For what is judged to be the thermally dominant state of S3, kT_{in} is higher than for the BH candidate systems. We therefore conclude that S3 and S5 are candidate Z-track sources.

The power law states do not show a bimodality as we see for the thermal states, but they are consistent with Galactic NS and BH XBs, and there appears some slight favoring of steeper Γ at lower luminosities. However, such an effect was also seen by Fabbiano et al. (2010), whose limiting luminosity for spectral fitting was much higher. In Figure 9 of Brassington et al. (2010) it is shown using 1000 count simulated spectra that the change in Γ with flux contribution favoured larger values from spectral fitting, particularly for cooler disks. It is conceivable that this effect becomes more pronounced when there are fewer counts.

4.2.1. *NS Transient Candidates*

Of the less luminous sources that do not appear to be BHCs we find that S25, S35 and S45 display extreme variability. S25 is only bright enough for spectral fitting in one observation, where we determine the source to be in a power law dominant state. While the source is always above our detection limit, the flux falls to $\sim 20\%$ of the initial value after obsID 7797, and the spectrum becomes dramatically softer

---

by obsID 8490, with $log_{10}(S/H) \sim 1.1$ and a 90% confidence lower-limit of ~ 0.6 in obsID 8490. That a source displays quasi-super-soft behavior (Di Stefano & Kong 2003) at low luminosity but $\Gamma \sim 2$ may indicate that S25 is a classical nova.

S35 is only detected in obsID 8490, but in fitting simple models we are not able to constrain N_H such as to show that it is above, below or consistent with N_H^{Gal}. All the parameters are poorly constrained, but taken at face value the Γ or kT_{in} are not inconsistent with NS LXMBs. The variability demonstrated by the source would be consistent with a transient atoll-type NS LMXB towards the peak of outburst.

We believe that S45 may also be a transient NS LMXB in outburst. It displays significant temporal variability over the course of the six observations, and appears to be in a thermally dominant state with an inner-disc temperature $kT_{in} \sim 1.3-2.3$ keV, consistent with disc temperatures obtained from Aql X-1 (e.g. Lin et al. 2007), which we suggest is an analogue to this source.

4.3. *S48: A high magnetic field NS in a GC?*

S48 is a peculiar source. Coincidence with a spectroscopically-confirmed GC means that it is highly unlikely to be a background AGN or foreground star. The spectrum is well-fit by a power law model of $\Gamma \sim 0.7$ experiencing negligible absorption, and a good fit cannot be achieved for the thermal model (Table 2). The luminosity of S48 makes it unlikely to be a cataclysmic variable, but it is similar to IGR J17361-4441, a hard X-ray transient detected by INTEGRAL in the Galactic globular cluster NGC 6388 (Ferrigno et al. 2011), which is possibly a high-magnetic field binary such as GX 1+4 (Paul et al. 2005), and has a similar power law slope. The spectra of these sources are well described by a cut-off power law of $\Gamma \sim 0.7-1.0$ with a high energy cut-off at 25 keV (Bozzo et al. 2011). The spectral shape is consistent with the compact object being a highly magnetized NS, the emission emanating from accretion columns that impact the NS surface. Young, highly magnetized radio pulsars have been observed in GCs by Boyles et al. (2011), so this is a plausible explanation. However, such sources typically show short-term modulation on a scale of a few hours (Corbet et al. 2008); while we do not detect any variability inside of any observation (Table 1), such modulation might be too small to be detected.

4.4. *Uncharacterised Spectral States*

There are a handful of examples of spectra that could not be formally distinguished by our method (Section 3.2). In the case of S29, S32, S34 and S36, we are able to determine the spectral state for a subset of the observations but not for others that we had previously shown to have a different spectral shape. In the case of S29, obsID 7798, the source may be experiencing an increase in absorption or some intermediate stage as it moves away from the hard state, as is the case with S34 obsID 8490. In obsIDs 7797, 7798 and 8490 of S36, we find N_H consistent with the N_H^{Gal} for both models. With the point estimate of N_H^{DBB} much closer to zero, we could tentatively suggest that this source remains in a power law dominated state throughout, the spectra becoming harder at certain times. We note that the softer state of this source coincides with its most luminous epoch, reminiscent of Galactic NS LMXBs such as 4U 1635-536, the spectra of which tend to harden as the source reaches its lowest outburst luminosities. In S31, there are two clear examples that seem to favor a thermal shape, but there is also clear evidence of a much harder

---

[21] Using the function *fitdistr*, part of the MASS package in R
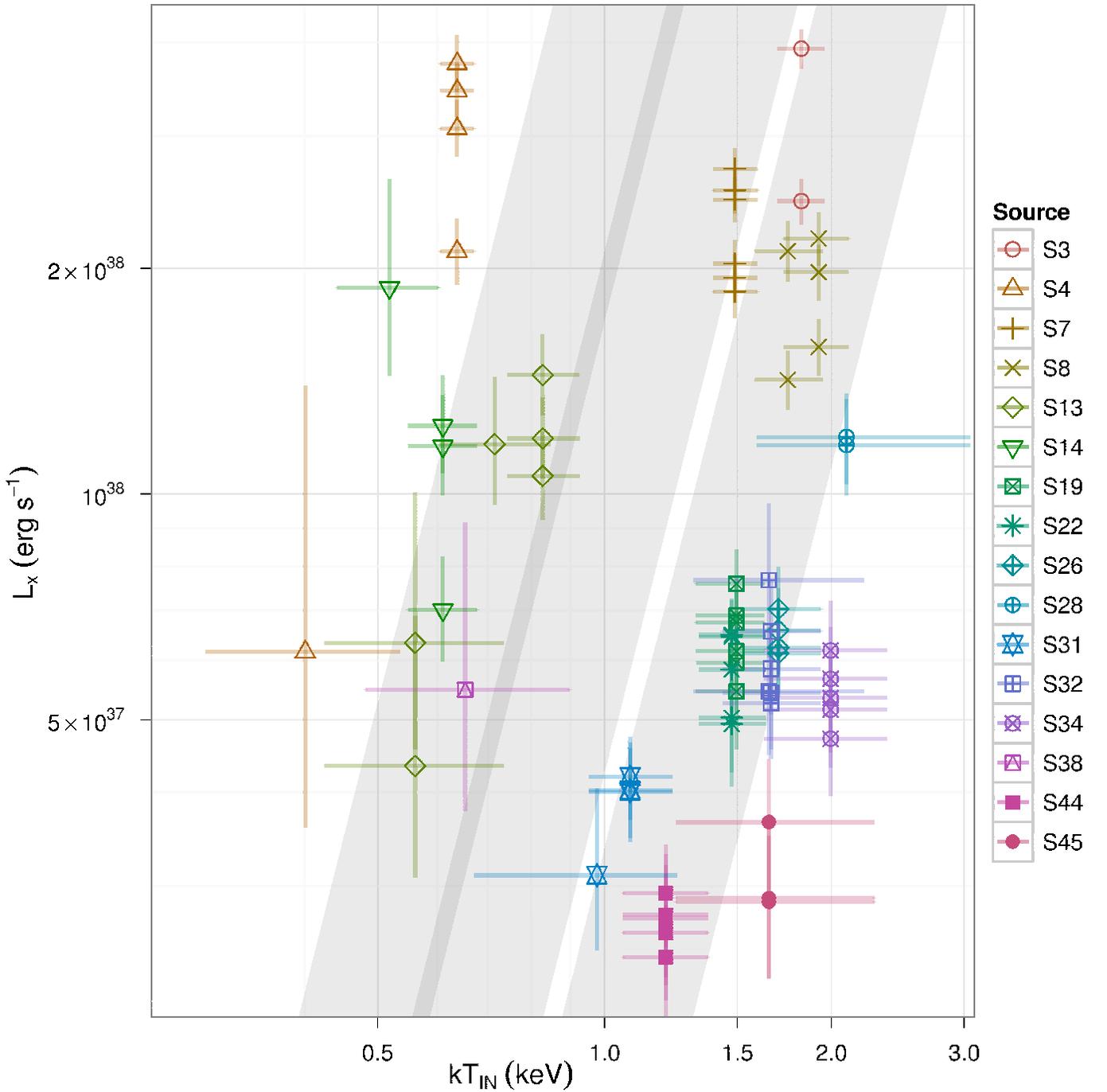
FIG. 2.— X-ray luminosity against inner-disk temperature for states deemed to be in the thermal state. Diagonal bands represent constant mass for (*left* to *right*) 10 $M_\odot$, 5 $M_\odot$ and 2 $M_\odot$ non-rotating compact objects. The width of the bands shows an assumed inclination θ of $\cos\theta = 0.25$ to $\cos\theta = 0.75$.

state in 0bsIDs 7798 & 8489 where it becomes more difficult for the fit to constrain the absorption column. For S32 obsID 8490, N_H could not be constrained for either simple model.

4.5. *A different population?*

Spectral fitting of simple models indicates that 6 of the 8 sources we highlight as being coincident with the dust lane (Table 1) experience a greater line-of-sight absorption than that provided by Galactic column alone. The two sources that were consistent with N_H^{Gal}, S34 and S46, are on the edge of the dust lane, they are thus the worst candidates for coincidence and were labeled as such out of caution. Of sources not co-

incident with the dust lane, only one source, S39, appears to experience excess absorption by our diagnostic. Inspection of the spectra of this source in more detail has led us to conclude that it is a background AGN, with a redshifted Fe line at ~ 4 keV present in the spectrum.

The good agreement between sources coincident with the dust lane and those that possess absorption surplus to the Galactic column strongly suggests that these sources experience additional absorption from the dust lane, and validates our previous analysis in section 4 using a K-band optical depth map to estimate of the average N_H in the vicinity of each source (with the exception of S24, which is not within
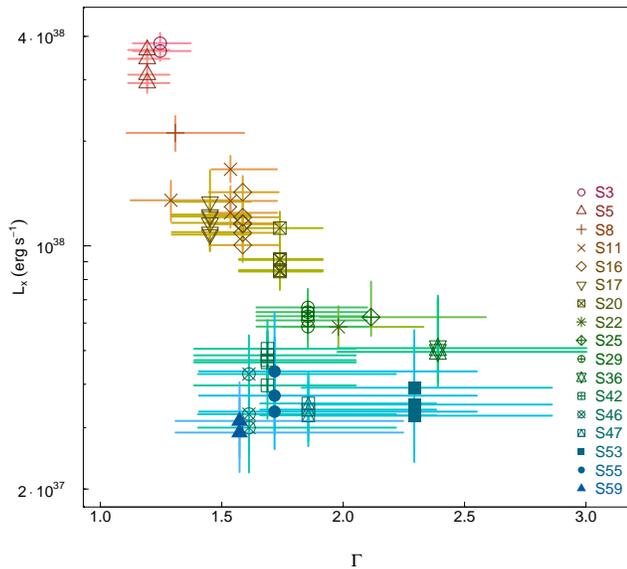
FIG. 3.— X-ray luminosity against photon index for those states determined to be power law dominated.

the FoV of the map), and then infer the dominant component in each of the spectra. This technique assumes that the sources are completely behind the dust lane, and that the N_H does not vary substantially over a $2''$ radius region, while in reality the material is likely to be clumpy and non-uniformly distributed.

Our four transient BH LMXB candidates are all dust lane sources, and are observed with $kT_{in} < 0.9$ keV. Two further dust lane systems, S12 & S28, possess very cool (< 0.4 keV) disks with a strong power law component, mildly suggesting that they also possess BHs. This result indicates an enhancement of classic BHC transients inside of the merged late-type galaxy relative to the halo. We note that previous studies identified the two known ULXs in the south-west quadrant of Cen A as transient X-ray binaries that are strong BHCs (e.g., Ghosh et al. 2006; Sivakoff et al. 2008). Although their presence strongly suggest that there is a population of transient BHCs outside of the merger region, neither source would have been identified as a transient based on the observations we consider in this paper. As such, we exclude them from our analysis.

Previously, hardness-intensity or color-color diagrams have been used to indicate which sources in a sample are heavily absorbed or not, but these were not ideal for giving an indication as to whether the sources themselves were similar, as any further difference in hardness or color could be ascribed to the additional (unknown and unconstrained) absorption. These results from detailed spectral fitting clearly point to particular types of source being present in the late-type galaxy that are absent from the rest of Cen A.

We propose a straightforward explanation of the lack of BHC transients outside of the late-type remnant. An empirical relation exists between orbital period and peak outburst luminosity (Wu et al. 2010), with larger luminosities produced by the systems with longer orbital periods. For transients that contain BHs, this luminosity exceeds 10^{38} erg s^{-1}, which corresponds to an orbital period of ~ 10 hours, based on the Wu et al. (2010) relation. For a main sequence companion

filling its Roche lobe, the mass m in M$_\odot$ will be related to the orbital period P in hours by $m \sim 0.11P$ (Frank et al. 2002), which means that the companion star must be be at *least* 1 M$_\odot$. It is likely that the donor is more evolved, particularly in a BH LMXB transient ($< 0.75M_{MS}$, King et al. 1996), and therefore the actual main sequence lifetime of the $\sim 1M_\odot$ donors is shorter. The majority (70-80%) of stars in the halo of Cen A were formed 12 ± 1 Gyr ago, with the rest formed from some event 8-10 Gyr later (Rejkuba et al. 2011). Therefore the majority of stars in the halo have $m < 1$M$_\odot$, which accounts for the relative absence of bright BH LMXB transients. Inside the late-type galaxy the star formation rate is at least 0.1 M$_\odot$ yr^{-1}, though could be as high as 1 M$_\odot$ yr^{-1} (Marconi et al. 2000); therefore there is a population of $\geq$ 1M$_\odot$ donors to feed the accreting BHs by Roche lobe overflow.

It has been proposed that the two ULXs in Cen A are BH LMXBs observed in the so-called *ultraluminous* state (e.g., Gladstone et al. 2009) at $L_x > 10^{39}$ erg s^{-1} and in quiescence with $L_x < 10^{36}$ erg s^{-1}. These sources have not been observed in the 'classic' BH LMXB states (Remillard & McClintock 2006) with L_x $10^{37} - 10^{39}$ erg s^{-1}; the non-UL outburst luminosity of these sources is unknown and therefore they should not be compared directly with the dust lane BHCs until they have been observed below 10^{39} erg s^{-1} but above the detectability threshold. In these relatively atypical sources, it is not yet clear how the orbital period and peak outburst luminosity are related, which complicates direct comparison with the dust lane sources.

If confirmed, the above explanation for the lack of BHC transients outside of the late-type remnant also accounts for the results of Kim & Fabbiano (2010) for a sample of other nearby early-type galaxies, who found the population of sources with $L_x > 4 \times 10^{38}$ erg s^{-1} diminished significantly with early-type age, a steepening of the discrete source XLF. We recommend population synthesis work be carried out to investigate the effects of a declining population of transient BH LMXBs with stellar age. We also suggest a deep monitoring campaign of other early-type galaxies with Chandra, to further investigate occurances of transient BHC XBs.

5. CONCLUSIONS

Our investigation into the X-ray binaries of Cen A has found:

i) The population is mostly NS LMXBs, with 6 BH candidates, four of which are inferred as such from the inner-disk temperature in the thermal state and inter-observational variability, and two from the inferred presence of a cool disk at a high luminosity. The proximity of Cen A, coupled with the depth of the VLP data, means that this is the only early-type galaxy where it is possible to perform detailed spectral fitting to sources in the classic XB luminosity range of $10^{37} - 10^{38}$ erg s^{-1}, similar to those sources we observe in the Milky Way. As a population of NS LMXBs outside of the Local Group, these are older analogues of sources that have been studied since the dawn of X-ray astronomy. We identify two sources that we suggest are Z track systems, based on their spectral shape, unabsorbed luminosity and persistent nature.

ii) There is some evidence that the mass distribution of compact objects is bimodal, and there is tentative evidence of the so-called 'mass gap' between $\sim 2.5 - 5M_\odot$ that has been observed in the population of Galactic transient LMXBs. This is the first time that the mass gap has been hinted at outside
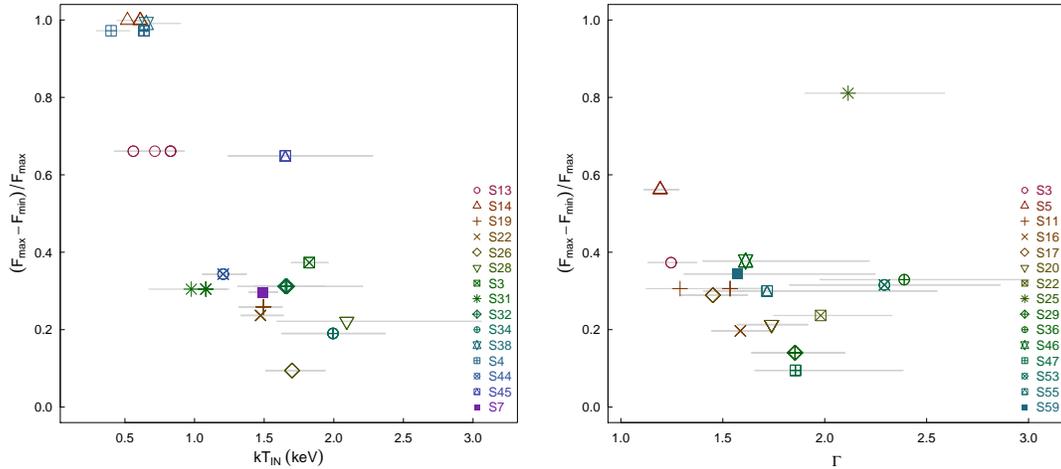
FIG. 4.— Inter-observation fractional variability against *(Left)* thermal state inner-disk temperatures and *(Right)* Power law state photon indices.

the Local Group.

iii) Besides the two known ULXs in Cen A, the only black hole candidate transient systems we can identify are found coincident with the dust lanes that arise from the merged late-type galaxy. These are four transient BH LMXB candidates observed in the thermal-dominant state. We propose that this is simply the result of stellar age; the older population of stars in the halo is unable to supply Roche lobe-filling companions that are required for the transient BHCs to have outburst peak $L_x > 10^{38}$erg s^{-1}. This also explains other recent results that show a steepening of the XLF of early-type galaxies with stellar age for $L_x > 4 - 5 \times 10^{38}$erg s^{-1} (Kim & Fabbiano 2010), as such sources would require more massive companions that have long since evolved off the main sequence. Similar analysis applied to other early-type galaxies where the ages of the stellar populations are known, coupled with stellar population synthesis work, is required to investigate the robustness of this explanation.

REFERENCES

Akaike, H. 1974, IEEE Transactions on Automatic Control, 19, 716
Angelini, L., Loewenstein, M., & Mushotzky, R. F. 2001, ApJ, 557, L35
Arnaud, K. A. 1996, in Astronomical Society of the Pacific Conference Series, Vol. 101, Astronomical Data Analysis Software and Systems V, ed. G. H. Jacoby & J. Barnes, 17
Bailyn, C. D., Jain, R. K., Coppi, P., & Orosz, J. A. 1998, ApJ, 499, 367
Belczynski, K., Wiktorowicz, G., Fryer, C. L., Holz, D. E., & Kalogera, V. 2012, ApJ, 757, 91
Boyles, J., Lorimer, D. R., Turk, P. J., et al. 2011, ApJ, 742, 51
Bozzo, E., Ferrigno, C., Stevens, J., et al. 2011, A&A, 535, L1
Brassington, N. J., Fabbiano, G., Blake, S., et al. 2010, ApJ, 725, 1805
Brassington, N. J., Fabbiano, G., Zezas, A., et al. 2012, ApJ, 755, 162
Burke, M. J., Raychaudhury, S., Kraft, R. P., et al. 2012, ApJ, 749, 112
Cappellari, M., Bacon, R., Bureau, M., et al. 2006, MNRAS, 366, 1126
Corbet, R. H. D., Sokoloski, J. L., Mukai, K., Markwardt, C. B., & Tueller, J. 2008, ApJ, 675, 1424
Coriat, M., Fender, R. P., & Dubus, G. 2012, MNRAS, 424, 1991
Croston, J. H., Kraft, R. P., Hardcastle, M. J., et al. 2009, MNRAS, 395, 1999
Di Stefano, R., & Kong, A. K. H. 2003, ApJ, 592, 884
Dickey, J. M., & Lockman, F. J. 1990, ARA&A, 28, 215
Dubus, G., Hameury, J.-M., & Lasota, J.-P. 2001, A&A, 373, 251
Fabbiano, G. 1989, ARA&A, 27, 87
—. 2006, ARA&A, 44, 323
Fabbiano, G., Brassington, N. J., Lentati, L., et al. 2010, ApJ, 725, 1824
Farr, W. M., Sravan, N., Cantrell, A., et al. 2011, ApJ, 741, 103
Fender, R. P., Belloni, T. M., & Gallo, E. 2004, MNRAS, 355, 1105
Ferrarese, L., Mould, J. R., Stetson, P. B., et al. 2007, ApJ, 654, 186
Ferrigno, C., Bozzo, E., Rodriguez, J., & Gibaud, L. 2011, The Astronomer's Telegram, 3566, 1

Frank, J., King, A., & Raine, D. J. 2002, Accretion Power in Astrophysics: Third Edition
Ghosh, K. K., Finger, M. H., Swartz, D. A., Tennant, A. F., & Wu, K. 2006, ApJ, 640, 459
Gierliński, M., & Done, C. 2004, MNRAS, 347, 885
Gladstone, J. C., Roberts, T. P., & Done, C. 2009, MNRAS, 397, 1836
Goodger, J. L., Hardcastle, M. J., Croston, J. H., et al. 2010, ApJ, 708, 675
Graham, J. A. 1979, ApJ, 232, 60
Gregory, P. C., & Loredo, T. J. 1992, ApJ, 398, 146
Grimm, H.-J., Gilfanov, M., & Sunyaev, R. 2002, A&A, 391, 923
Güver, T., & Özel, F. 2009, MNRAS, 400, 2050
Hardcastle, M. J., Kraft, R. P., Sivakoff, G. R., et al. 2007, ApJ, 670, L81
Harris, G. L. H., Gómez, M., Harris, W. E., et al. 2012, AJ, 143, 84
Harris, W. E., Spitler, L. R., Forbes, D. A., & Bailin, J. 2010, MNRAS, 401, 1965
Homan, J., Wijnands, R., van der Klis, M., et al. 2001, ApJS, 132, 377
Jordán, A., Sivakoff, G. R., McLaughlin, D. E., et al. 2007, ApJ, 671, L117
Kainulainen, J. T., Alves, J. F., Beletsky, Y., et al. 2009, A&A, 502, L5
Kim, D.-W., & Fabbiano, G. 2004, ApJ, 611, 846
—. 2010, ApJ, 721, 1523
King, A. R., Kolb, U., & Burderi, L. 1996, ApJ, 464, L127
King, I. 1962, AJ, 67, 471
Kraft, R. P., Hardcastle, M. J., Sivakoff, G. R., et al. 2008, ApJ, 677, L97
Kreidberg, L., Bailyn, C. D., Farr, W. M., & Kalogera, V. 2012, ApJ, 757, 36
Kundu, A., Maccarone, T. J., & Zepf, S. E. 2002, ApJ, 574, L5
Lin, D., Remillard, R. A., & Homan, J. 2007, ApJ, 667, 1073
Lin, D., Remillard, R. A., Homan, J., & Barret, D. 2012, ApJ, 756, 34
Maccarone, T. J. 2003, A&A, 409, 697
Maccarone, T. J., & Coppi, P. S. 2003, A&A, 399, 1151

Maccarone, T. J., Kundu, A., Zepf, S. E., & Rhode, K. L. 2007, Nature, 445, 183

Marconi, A., Schreier, E. J., Koekemoer, A., et al. 2000, ApJ, 528, 276

Paul, B., Dotani, T., Nagase, F., Mukherjee, U., & Naik, S. 2005, ApJ, 627, 915

Portegies Zwart, S. F., Dewi, J., & Maccarone, T. 2004, MNRAS, 355, 413

Prestwich, A. H., Kilgard, R. E., Primini, F., McDowell, J. C., & Zezas, A. 2009, ApJ, 705, 1632

Quillen, A. C., Brookes, M. H., Keene, J., et al. 2006, ApJ, 645, 1092

Raymond, J. C., & Smith, B. W. 1977, ApJS, 35, 419

Rejkuba, M., Harris, W. E., Greggio, L., & Harris, G. L. H. 2011, A&A, 526, A123

Remillard, R. A., & McClintock, J. E. 2006, ARA&A, 44, 49

Roberts, T. P., Levan, A. J., & Goad, M. R. 2008, MNRAS, 387, 73

Sarazin, C. L., Irwin, J. A., & Bregman, J. N. 2000, ApJ, 544, L101

—. 2001, ApJ, 556, 533

Shahbaz, T., Charles, P. A., & King, A. R. 1998, MNRAS, 301, 382

Shakura, N. I., & Sunyaev, R. A. 1973, A&A, 24, 337

Shih, I. C., Kundu, A., Maccarone, T. J., Zepf, S. E., & Joseph, T. D. 2010, ApJ, 721, 323

Sivakoff, G. R., Kraft, R. P., Jordán, A., et al. 2008, ApJ, 677, L27

Smak, J. 1984, PASP, 96, 5

Thorne, K. S., & Price, R. H. 1975, ApJ, 195, L101

van der Klis, M. 1994, ApJS, 92, 511

van Haaften, L. M., Nelemans, G., Voss, R., Wood, M. A., & Kuijpers, J. 2012, A&A, 537, A104

Voss, R., Gilfanov, M., Sivakoff, G. R., et al. 2009, ApJ, 701, 471

Weisskopf, M. C., Tananbaum, H. D., Van Speybroeck, L. P., & O'Dell, S. L. 2000, in Society of Photo-Optical Instrumentation Engineers (SPIE) Conference Series, Vol. 4012, Society of Photo-Optical Instrumentation Engineers (SPIE) Conference Series, ed. J. E. Truemper & B. Aschenbach, 2–16

White, N. E., & Marshall, F. E. 1984, ApJ, 281, 354

Whittet, D. C. B. 1992, Dust in the galactic environment

Worrall, D. M., Birkinshaw, M., Kraft, R. P., et al. 2008, ApJ, 673, L135

Wu, Y. X., Yu, W., Li, T. P., Maccarone, T. J., & Li, X. D. 2010, ApJ, 718, 620

Zhang, S. N., Cui, W., & Chen, W. 1997, ApJ, 482, L155

Zhang, Z., Gilfanov, M., Voss, R., et al. 2011, A&A, 533, A33

TABLE 3
CEN A SOURCES: SPECTRAL FITTING AND STATE IDENTIFICATION

Source	ObsIDs	N_H^{PO} 10^{22} cm^{-2}	Γ^{PO}	L_x (0.5-10.0 keV)^{PO} 10^{37} erg s^{-1}	χ^2/dof	N_H^{DBB} 10^{22} cm^{-2}	kT_{in}^{DBB} keV	L_x (0.5-10.0 keV)^{DBB} 10^{37} erg s^{-1}	χ^2/dof	State
S3	7797,7800	$0.13^{0.08}_{0.07}$	$1.25^{0.13}_{0.12}$	$36.2^{2.4}_{2.3}, 38.2^{2.7}_{2.6}$	109.6/117	$0.00^{0.05}_{0.00}$	$2.61^{0.32}_{0.35}$	$30.3^{2.5}_{2.3}, 31.7^{2.9}_{2.7}$	106.7/117	P1
S3	8489,8490	$0.21^{0.07}_{0.06}$	$1.50^{0.11}_{0.11}$	$31.7^{2.1}_{2.0}, 50.7^{2.8}_{2.7}$	131/140	$0.04^{0.05}_{0.04}$	$1.92^{0.21}_{0.17}$	$24.5^{1.8}_{1.7}, 39.2^{2.5}_{2.4}$	118.6/140	T1
S4	7797,7798,7799,7800	$1.25^{0.11}_{0.1}$	$3.76^{0.19}_{0.18}$	$93.77^{24.83}_{18.44}, 166.21^{42.48}_{31.51}$	241.2/203	$0.65^{0.07}_{0.06}$	$0.64^{0.03}_{0.03}$	$21.06^{2.23}_{2.04}, 37.49^{3.41}_{3.09}$	206.9/203	I
S4	8489	$1.22^{0.7}_{0.51}$	$5.07^{1.69}_{1.22}$	62^{447}_{46}	10.5/14	$0.59^{0.48}_{0.35}$	$0.40^{0.13}_{0.11}$	$6.15^{7.79}_{2.57}$	10.0/14	I
S5	7797,7800,8489,8490	$0.11^{0.05}_{0.05}$	$1.19^{0.09}_{0.09}$	$29.4^{1.9}_{1.9}, 36.6^{2.3}_{2.2}$	180/214	$0.00^{0.00}_{-0.82}$	$2.83^{0.31}_{0.25}$	$24.9^{1.9}_{1.8}, 31.1^{2.4}_{2.2}$	185.7/214	P1,N
S7	7797,7798,7799,8490,7800,8489	$0.89^{0.1}_{0.1}$	$1.99^{0.12}_{0.11}$	$28.8^{2.8}_{2.6}, 42.0^{3.8}_{3.4}$	275.7/256	$0.51^{0.07}_{0.06}$	$1.49^{0.11}_{0.1}$	$18.6^{1.5}_{1.4}, 27.2^{1.8}_{1.8}$	271.5/256	I
S8	7797,7798,8490	$0.29^{0.08}_{0.08}$	$1.58^{0.14}_{0.13}$	$20.6^{1.66}_{1.62}, 28.44^{2.14}_{2.07}$	128/132	$0.08^{0.05}_{0.05}$	$1.93^{0.25}_{0.21}$	$15.71^{1.41}_{1.34}, 21.91^{1.85}_{1.76}$	135.7/132	T1
S8	7799	$0.06^{0.16}_{0.06}$	$1.31^{0.28}_{0.2}$	$21.11^{2.52}_{2.37}$	23.2/34	$0.00^{0.00}_{-0.82}$	$2.07^{0.57}_{0.38}$	$16.8^{2.8}_{2.4}$	27.6/34	P1,N
S8	7800,8489	$0.23^{0.10}_{0.09}$	$1.57^{0.17}_{0.16}$	$18.6^{1.56}_{1.51}, 27.58^{2.26}_{2.20}$	87.6/87	$0.04^{0.06}_{0.04}$	$1.87^{0.3}_{0.23}$	$14.19^{1.37}_{1.29}, 21.07^{2.12}_{1.96}$	87.8/87	T1
S11	7797	$0.07^{0.18}_{0.07}$	$1.26^{0.32}_{0.23}$	$13.5^{1.9}_{1.8}$	17.3/23	$0.00^{0.00}_{-0.82}$	$2.19^{0.74}_{0.45}$	$10.8^{2.1}_{1.7}$	17.8/23	P1,N
S11	7800,8489,8490	$0.09^{0.11}_{0.09}$	$1.54^{0.19}_{0.18}$	$12.4^{1.4}_{1.3}, 16.6^{1.5}_{1.5}$	72.3/73	$0.00^{0.00}_{-0.82}$	$1.66^{0.20}_{0.15}$	$9.52^{1.15}_{1.07}, 12.5^{1.4}_{1.2}$	83/73	P1,N
S12	7797,7798,7799,7800,8489,8490	$0.72^{0.21}_{0.19}$	$1.12^{0.18}_{0.17}$	$16.35^{1.88}_{1.85}, 26.54^{2.34}_{2.29}$	150.8/157	$0.49^{0.13}_{0.12}$	$3.96^{1.73}_{0.87}$	$14.49^{1.91}_{1.79}, 23.5^{2.5}_{2.3}$	153.6/157	I
S13	S7797,7798,8490	$0.9^{0.2}_{0.18}$	$2.97^{0.31}_{0.29}$	$27.05^{10.35}_{6.46}, 36.85^{13.55}_{8.44}$	122/89	$0.4^{0.13}_{0.12}$	$0.83^{0.11}_{0.09}$	$10.57^{1.53}_{1.33}, 14.41^{1.93}_{1.69}$	110.7/89	I
S13	7800,8489	$1.02^{0.57}_{0.44}$	$3.99^{1.16}_{0.89}$	$22.53^{67.86}_{13.54}, 33^{100.31}_{19.79}$	41.3/30	$0.39^{0.37}_{0.29}$	$0.56^{0.17}_{0.14}$	$4.34^{2.55}_{1.26}, 6.33^{3.72}_{1.77}$	37.5/30	I
S13	7799	$0.85^{0.34}_{0.27}$	$3.33^{0.61}$	$35.79^{33.25}_{13.48}$	58.2/33	$0.35^{0.21}_{0.17}$	$0.71^{0.13}_{0.11}$	$11.65^{2.68}_{1.97}$	44.9/33	I
S14	7797,7798,7800	$0.95^{0.19}_{0.17}$	$3.81^{0.39}_{0.35}$	$31.4^{17.7}_{10.0}, 55.4^{30.7}_{17.4}$	78.1/71	$0.37^{0.12}_{0.11}$	$0.61^{0.07}_{0.06}$	$7.00^{1.24}_{1.03}, 12.33^{2.07}_{1.68}$	72/71	I
S14	7799	$1.65^{0.46}_{0.37}$	$4.66^{0.78}_{0.64}$	192^{356}_{108}	19.9/27	$0.81^{0.28}_{0.23}$	$0.52^{0.08}_{0.08}$	$18.8^{7.4}_{4.4}$	14.6/27	I
S16	7797,7798,7799,7800,8489,8490	$0.14^{0.08}_{0.08}$	$1.59^{0.15}_{0.14}$	$10.0^{1.1}_{1.1}, 14.3^{1.6}_{1.6}$	126.5/129	$0.00^{0.00}_{-0.82}$	$1.67^{0.16}_{0.14}$	$7.50^{0.86}_{0.83}, 10.5^{1.3}_{1.2}$	133.7/129	P1,N
S17	7797,7798,7799,7800,8489,8490	$0.16^{0.11}_{0.10}$	$1.45^{0.17}_{0.16}$	$10.77^{1.16}_{1.13}, 13.4^{3.1}_{3.0}$	93.1/105	$0.00^{0.06}_{0.00}$	$1.98^{0.24}_{0.17}$	$8.21^{0.8}_{0.94}, 10.28^{2.26}_{2.25}$	92.5/105	P1
S19	7797,7798,7799,7800,8489,8490	$0.35^{0.13}_{0.11}$	$1.84^{0.2}_{0.19}$	$7.91^{1.37}_{1.31}, 11.08^{1.36}_{1.23}$	121/135	$0.09^{0.08}_{0.07}$	$1.5^{0.21}_{0.17}$	$5.45^{0.92}_{0.89}, 7.59^{0.85}_{0.82}$	119.3/135	T1
S20	7797,7798,7799,8489,8490,7800	$0.17^{0.1}_{0.09}$	$1.74^{0.18}_{0.17}$	$8.43^{0.98}_{0.95}, 11.25^{1.30}_{1.24}$	83.5/113	$0.00^{0.00}_{-0.82}$	$1.45^{0.14}_{0.12}$	$5.98^{0.72}_{0.69}, 7.94^{0.94}_{0.89}$	90.2/113	P1,N
S22	7797	$0.0^{0.2}_{0.0}$	$1.82^{0.46}$	$5.61^{1.00}_{0.78}$	12.9/14	$0.00^{0.00}_{-0.82}$	$1.16^{0.28}_{0.23}$	$4.21^{0.74}_{0.66}$	20.9/14	P1,N
S22	7798,7799,7800,8489,8490	$0.21^{0.13}_{0.12}$	$1.7^{0.22}_{0.21}$	$6.90^{0.93}_{0.90}, 8.83^{1.07}_{1}$	60.1/67	$0.00^{0.00}_{-0.82}$	$1.62^{0.19}_{0.16}$	$4.94^{0.74}_{0.69}, 6.40^{0.78}_{0.74}$	60/67	T2,M3,I
S24	7797	$0.36^{0.4}_{0.33}$	$1.54^{0.52}_{0.47}$	$10.68^{2.11}_{1.62}$	9.4/14	$0.13^{0.26}_{0.13}$	$1.85^{1.12}_{0.52}$	$7.80^{1.75}_{1.34}$	8.6/14	NA
S24	7798,7799,7800,8489	$0.64^{0.28}_{0.25}$	$1.72^{0.3}_{0.27}$	$10.4^{1.9}_{1.5}, 12.8^{2.4}_{1.8}$	74.8/67	$0.33^{0.18}_{0.16}$	$1.68^{0.38}_{0.27}$	$7.31^{0.96}_{0.92}, 9.03^{1.21}_{1.15}$	67.2/67	I
S25	7797	$0.11^{0.21}_{0.11}$	$2.11^{0.47}_{0.36}$	$6.24^{1.66}_{1.08}$	14/15	$0.00^{0.00}_{-0.82}$	$1^{0.18}_{0.15}$	$4.28^{0.59}_{0.56}$	14.1/15	P1,N
S26	7797,7798,7799,7800	$0.22^{0.13}_{0.12}$	$1.57^{0.21}_{0.20}$	$8.29^{1}_{0.98}, 9.38^{1.17}_{1.13}$	49.1/60	$0.02^{0.09}_{0.02}$	$1.84^{0.32}_{0.25}$	$6.14^{0.92}_{0.85}, 7.03^{1}_{0.92}$	50.3/60	T1
S28	7797,8490	$0.51^{0.53}_{0.48}$	$0.87^{0.41}_{0.39}$	$1.20^{1.78}_{1.67}, 17.07^{2.54}_{2.38}$	17.5/27	$0.44^{0.36}_{0.30}$	$5.60^{NA}_{2.72}$	$11.1^{2.43}_{1.94}, 15.74^{3.54}_{2.80}$	17.0/31	I
S28	7800,8489	$1.66^{0.72}_{0.64}$	$1.71^{0.49}_{0.45}$	$16.58^{6.19}_{3.21}, 16.95^{6.58}_{3.3}$	36.7/28	$1.10^{0.45}_{0.4}$	$2.09^{0.97}_{0.5}$	$11.62^{1.76}_{1.66}, 11.9^{1.7}_{1.1}$	34.8/28	I
S29	7797,7799,7800,8489,8490	$0.16^{0.12}_{0.11}$	$1.85^{0.24}_{0.23}$	$5.86^{0.81}_{0.76}, 6.65^{0.87}_{0.82}$	65.1/64	$0.00^{0.00}_{-0.82}$	$1.28^{0.15}_{0.13}$	$4.00^{0.55}_{0.53}, 4.45^{0.62}_{0.58}$	80.2/64	P1,N
S29	7798	$0.83^{0.50}_{0.39}$	$2.55^{0.65}_{0.55}$	$10.30^{8.80}_{3.30}$	9/10	$0.38^{0.32}_{0.26}$	$1.04^{0.32}_{0.22}$	$5.14^{1.24}_{0.96}$	8/10	I
S31	7797,7800,8490	$0.26^{0.17}_{0.15}$	$2.08^{0.34}_{0.31}$	$6.23^{1.19}_{0.93}, 6.51^{1.25}_{0.95}$	30/43	$0.00^{0.09}_{0.00}$	$1.20^{0.11}_{0.18}$	$3.91^{0.59}_{0.45}, 4.09^{0.56}_{0.47}$	37.4/43	T1
S31	7798,8489	$0.00^{0.82}_{0.00}$	$1.29^{0.20}_{0.19}$	$6.31^{1.80}_{1.37}, 6.69^{1.00}_{1.11}$	21.3/27	$0.00^{0.82}_{0.00}$	$1.85^{0.66}_{0.40}$	$4.72^{1.10}_{0.86}, 5.17^{1.35}_{1.00}$	24.5/27	NA
S31	7799	$0.53^{0.60}_{0.43}$	$2.58^{1.06}_{0.77}$	$6.24^{9.34}_{2.22}$	13.7/12	$0.12^{0.38}_{0.12}$	$0.98^{0.58}_{0.31}$	$3.10^{0.94}_{0.74}$	13.3/12	T1
S32	7797,7798,7799,7800	$0.26^{0.18}_{0.16}$	$1.61^{0.28}_{0.26}$	$7.22^{1.16}_{1.09}, 8.98^{1.32}_{1.25}$	26.5/50	$0.03^{0.12}_{0.03}$	$1.79^{0.36}_{0.32}$	$5.27^{0.94}_{0.85}, 6.58^{1.13}_{1.01}$	27.5/50	T1
S32	8489,8490	$0.00^{0.00}_{-0.82}$	$1.32^{0.23}_{0.22}$	$7.18^{1.35}_{1.21}, 10.61^{2.39}_{2.1}$	13/16	$0.00^{0.00}_{-0.82}$	$1.8^{0.69}_{0.40}$	$5.45^{1.30}_{1.03}, 7.75^{2.21}_{1.71}$	14.3/16	T2,M3,I,N,M2
S34	7797,7798,7799,7800,8489	$0.32^{0.18}_{0.16}$	$1.55^{0.26}_{0.24}$	$6.23^{0.96}_{0.93}, 8.14^{1.13}_{1.08}$	48.2/67	$0.08^{0.12}_{0.08}$	$2.00^{0.58}_{0.37}$	$4.72^{0.84}_{0.76}, 6.19^{1.03}_{0.92}$	52.6/67	T1

TABLE 3 — *Continued*

Source	ObsIDs	N_H^{PO} 10^{22} cm^{-2}	Γ^{PO}	L_x (0.5−10.0 keV)^{PO} 10^{37} erg s^{-1}	χ^2/dof	N_H^{DBB} 10^{22} cm^{-2}	kT_{in}^{DBB} keV	L_x (0.5−10.0 keV)^{DBB} 10^{37} erg s^{-1}	χ^2/dof	State
S34	8490	$0.97^{0.55}_{0.43}$	$2.26^{0.62}_{0.52}$	$11.34^{7.61}_{3.03}$	8.5/13	$0.49^{0.34}_{0.27}$	$1.32^{0.46}_{0.3}$	$6.46^{1.23}_{1.11}$	7.3/13	I
S35	8490	$0.51^{0.6}_{0.49}$	$1.81^{0.74}_{0.66}$	$8.02^{4.0}_{1.54}$	7.1/10	$0.20^{0.40}_{0.20}$	$1.49^{1.05}_{0.47}$	$5.28^{1.28}_{0.98}$	6.9/10	NA
S36	7797, 7798, 8490	$0.20^{0.21}_{0.18}$	$1.54^{0.36}_{0.34}$	$4.5^{0.94}_{0.86}, 7.31^{1.14}_{1.06}$	30.5/31	$0.02^{0.14}_{0.02}$	$1.71^{0.46}_{0.38}$	$3.20^{0.82}_{0.66}, 5.17^{1.09}_{0.87}$	29.7/31	NA
S36	7799, 7800	$0.20^{0.23}_{0.20}$	$2.39^{0.61}_{0.50}$	$4.96^{2.11}_{1.04}, 5.08^{2.11}_{1.04}$	23.8/23	$0.00^{0.00}_{-0.82}$	$0.87^{0.19}_{0.15}$	$2.85^{0.49}_{0.45}, 2.92^{0.50}_{0.45}$	33.4/23	P1,N
S38	8490	$1.41^{0.76}_{0.64}$	$3.87^{1.25}_{1.00}$	$31.34^{126.4}_{20.9}$	6.1/9	$0.60^{0.52}_{0.43}$	$0.65^{0.25}_{0.17}$	$5.48^{3.68}_{1.70}$	7.8/9	I
S39	7797, 7798, 7799	$0.93^{0.43}_{0.38}$	$1.98^{0.48}_{0.44}$	$7.05^{2.65}_{1.44}, 9.28^{3.42}_{1.9}$	37.2/30	$0.41^{0.27}_{0.24}$	$1.65^{0.65}_{0.38}$	$4.45^{0.79}_{0.73}, 5.80^{1.06}_{0.96}$	41.3/30	I
S39	7799, 7800, 8490	$0.92^{0.45}_{0.37}$	$2.34^{0.53}_{0.47}$	$8.11^{4.8}_{2.22}, 10.085^{5.64}_{2.71}$	19.6/26	$0.43^{0.29}_{0.24}$	$1.20^{0.36}_{0.24}$	$4.28^{0.90}_{0.79}, 5.46^{1.16}_{1.07}$	21.3/26	I
S42	7797, 7799, 7800, 8489, 8490	$0.13^{0.22}_{0.13}$	$1.69^{0.36}_{0.30}$	$3.97^{0.87}_{0.79}, 5.06^{1.06}_{0.99}$	46.5/44	$0.00^{0.00}_{-0.82}$	$1.38^{0.25}_{0.19}$	$2.78^{0.58}_{0.54}, 3.54^{0.78}_{0.71}$	44.7/44	P1,N
S44	7797, 7799, 7800, 8489, 8490	$0.30^{0.20}_{0.18}$	$2.03^{0.34}_{0.31}$	$3.71^{0.84}_{0.67}, 4.37^{1.05}_{0.81}$	30.2/42	$0.01^{0.13}_{0.01}$	$1.30^{0.22}_{0.21}$	$2.37^{0.42}_{0.40}, 2.83^{0.50}_{0.42}$	28.4/42	T1
S45	7798, 7800, 8490	$0.48^{0.39}_{0.32}$	$1.76^{0.49}_{0.44}$	$4.07^{1.37}_{0.91}, 5.19^{1.51}_{1.02}$	27.7/21	$0.18^{0.26}_{0.18}$	$1.65^{0.77}_{0.36}$	$2.86^{0.65}_{0.60}, 3.65^{0.78}_{0.70}$	28.5/21	T1
S46	7797, 8489, 8490	$0.11^{0.45}_{0.11}$	$1.61^{0.61}_{0.32}$	$3.00^{0.99}_{0.81}, 4.28^{1.25}_{0.95}$	28.2/27	$0.00^{0.21}_{0.00}$	$1.51^{0.48}_{0.36}$	$2.16^{0.70}_{0.57}, 3.13^{0.84}_{0.70}$	26.3/27	P1
S47	7797, 8489, 8490	$0.11^{0.26}_{0.11}$	$1.86^{0.53}_{0.35}$	$3.26^{0.82}_{0.63}, 3.52^{0.79}_{0.68}$	14.7/23	$0.00^{0.00}_{-0.82}$	$1.13^{0.26}_{0.19}$	$2.16^{0.45}_{0.40}, 2.32^{0.53}_{0.45}$	17.3/23	P1,N
S48	7798, 8490, 7799	$0.00^{0.00}_{-0.82}$	$0.75^{0.22}_{0.22}$	$5.17^{1.49}_{1.24}, 6.97^{1.45}_{1.31}$	12.8/18	NA^{NA}_{NA}	NA^{NA}_{NA}	NA, NA	NA/NA	M2
S53	7797, 7800, 8490	$0.30^{0.32}_{0.28}$	$2.29^{0.57}_{0.49}$	$3.25^{1.66}_{0.86}, 3.91^{1.81}_{0.93}$	16/19	$0.00^{0.00}_{-0.82}$	$1.07^{0.21}_{0.17}$	$1.93^{0.37}_{0.35}, 2.28^{0.45}_{0.43}$	17.8/19	P1,N
S55	7797, 7798, 7799	$0.19^{0.59}_{0.19}$	$1.72^{0.83}_{0.45}$	$3.34^{1.55}_{0.75}, 4.36^{2.05}_{1.01}$	15.1/14	$0.00^{0.00}_{-0.82}$	$1.42^{0.53}_{0.32}$	$2.27^{0.65}_{0.52}, 2.94^{0.9}_{0.68}$	17/14	P1,N
S59	8489, 8490	$0.11^{0.42}_{0.11}$	$1.57^{0.67}_{0.39}$	$2.91^{0.74}_{0.68}, 3.14^{0.92}_{0.81}$	9.8/12	$0.00^{0.00}_{-0.82}$	$1.55^{0.74}_{0.41}$	$2.07^{0.67}_{0.52}, 2.3^{0.83}_{0.62}$	10.6/12	P1,N

NOTE. — Results from fitting absorbed power law (*PO*) and disk blackbody (*DBB*) models with all parameters free to vary and 95% confidence intervals. The state column denotes the spectral states that a given set of spectra are consistent with, based on the classification scheme proposed by Brassington et al. (2010). T indicates a thermally dominant state, P indicates power law dominant state, M suggests that there is significant, unmodelled emission from another component ($> 30-40\%$), N suggests a result was not-produced by the Brassington et al. (2010) simulations and I indicates there is additional line-of-sight absorption, when both simple models have N_H significantly above the Galactic value. The extent to which a component dominates is indicated by the associated number, i.e. 1 implies the state is almost completely dominated by that component, while 2 indicates that there is some unmodelled component also present. Instances of $N_H^{DBB} = 0.00^{0.00}_{-0.82}$ for some fits are the result of not being able to constrain an upper-limit in Xspec. We believe the source to be in the power law state at these times, with N_H^{PO} consistent with the Galactic value. In the state column, 'NA' denotes where no inference can be made regarding the state (see section 4.4) and for S48 shows where no fit could be achieved (i.e. $\chi/dof > 2$), which is discussed in section 4.3.

[a] Minimal and maximal values of L_x are shown for absorbed power law (PO) and disk blackbody (DBB) models